Doctoral theses at NTNU, 2022:346

Taekwang Ha

On measuring, prediction and control of 3D profile bending towards Industry 4.0

Doctoral thesis

NTNU
Norwegian University of Science and Technology
Thesis for the Degree of Philosophiae Doctor
Faculty of Engineering
Department of Mechanical and Industrial Engineering
Texas A&M University
Department of Multidisciplinary Engineering

NTNU
Norwegian University of Science and Technology

TEXAS A&M UNIVERSITY

Taekwang Ha

On measuring, prediction and control of 3D profile bending towards Industry 4.0

Thesis for the Degree of Philosophiae Doctor

Trondheim, January 2023

Norwegian University of Science and Technology
Faculty of Engineering
Department of Mechanical and Industrial Engineering

Texas A&M University
Department of Multidisciplinary Engineering

NTNU
Norwegian University of Science and Technology

Thesis for the Degree of Philosophiae Doctor

Faculty of Engineering
Department of Mechanical and Industrial Engineering

Texas A&M University
Department of Multidisciplinary Engineering

ISBN 978-82-326-6275-3 (printed ver.)
ISBN 978-82-326-5601-1 (electronic ver.)
ISSN 1503-8181 (printed ver.)
ISSN 2703-8084 (online ver.)

Doctoral theses at NTNU, 2022:346

Printed by NTNU Grafisk senter

Preface

This doctoral thesis is submitted to the Norwegian University of Science and Technology (NTNU) in partial fulfillment of the requirements for the dual degree of Doctor of Philosophy. This work of the Ph.D. thesis was carried out at the Department of Mechanical and Industrial Engineering (MTP) of NTNU in Trondheim, Norway and the Department of Multidisciplinary Engineering (MTDE) of Texas A&M University (TAMU) in College Station, USA. As a part of the dual Ph.D. degree program between TAMU and NTNU this work herein was accomplished under the supervision of Professor Torgeir Welo and Professor Geir Ringen of NTNU, and Professor Jyhwen Wang of TAMU.

This work was financially and infrastructurally supported by NTNU under the strategy of Digital Transformation – and the sub-project Rational Alloy Design (ALLDESIGN; ID: 2505257), the NTNU Aluminium Product Innovation Center (NAPIC), and the Research Council of Norway under Grant Number 267768. The advanced computing resources provided by Texas A&M High Performance Research Computing (HPRC) were used to finite element simulations.

Abstract

Aluminum profile bending is one of the methods providing potential to reduce weight and improve fuel efficiency in automotive, aerospace, and other industries. Most of manufacturers make efforts to reduce the number of components and processing steps for manufacturing efficiency and to increase product quality. Two and three-dimensional shapes of products are also demanded to satisfy aesthetic perspectives.

To meet the industrial demands toward Industry 4.0, the current research mainly focuses on the development of the springback monitoring and control by non-contact measurement methods, analytic models and artificial neural networks. A new strategy for on-machine springback measurement in rotary draw bending was developed. The measurement strategy is to evaluate springback by integrating digital image processing and laser tracking, enabling the bending process and springback to be monitored in real time. As a non-contact measurement method, this affordable system eliminates an offline measurement process by integrative monitoring the springback angle in rotary draw bending.

Based on the digital image measurement strategy in rotary draw bending, an in-situ springback monitoring technique was also developed for stretch bending of large-size profiles. The measurement technique is to evaluate springback in real time. Using the so-called circular hough transform algorithm, the center of reference circles marked on the profile were detected, and springback was calculated. The applicability of computer vision-based springback monitoring in large-size profile bending was validated with experiments.

In advanced 3D stretch bending, a 5-axis machine was used to bend hollow aluminum alloy profiles. The method provides the capability of reduced springback for complex shapes. The configuration of the 3D bend die and its rotational mechanism were kinematically analyzed and an analytical springback model was proposed based on the Frenet-Serret theorem. While the kinematically controlled stretch bending imposes stretch through the configuration of the tool, super-imposed stretch applied prior to bending provides further springback reduction. Thus, the effect of the pre-stretch before bending was also explored in this work. The proposed model was validated with finite element simulations and experiments to demonstrate springback evaluation for product design and process control purposes.

To reduce springback variations and improve process control, an artificial neural network (ANN) model was developed. The ANN model was trained based on experimental and analytical data. This model provides compensated bending angles to achieve the desired dimensions of the product. The proposed strategy was validated with 2D and 3D stretch bending experiments and provided evidence to improve the dimensional quality of bent profiles.

Dedication

To my parents, my wife Hyejung Han, and my son Noah Ha for their encouragement.

Acknowledgments

I would like to express my deepest gratitude to Dr. Jyhwen as the committee chair at TAMU and the co-supervisor at NTNU; Dr. Torgeir Welo as the main-supervisor at NTNU and the co-chair at TAMU; and Dr. Geir Ringen as the co-supervisor at NTNU and my committee member at TAMU. Dr. Wang always encouraged and guided me when I lost my way to go. Dr. Welo financially supported the dual degree Ph.D. program for me and provided the overall directions and feedback on my research. Dr. Ringen also supported the dual Ph.D. degree program and made efforts to manage this research program in the front line. Without their true support, guidance and feedback amidst the pandemic, I could not have accomplished this dual Ph.D. degree program between TAMU and NTNU.

I would like to acknowledge my friends and colleagues in Norway, Drs. Jun Ma, Jørgen Blindheim, and Sigmund Tronvoll for their suggestions and assisting with the experiments at NTNU. Without their effort, my research papers and this dissertation would not have been successful. Thanks also go to the department faculty and staff for making my time at TAMU and NTNU.

Finally, thanks to my father, who passed away during my Ph.D. education, my mother, my younger brother and sister, and my parent-in-law for their continuous encouragement. I would also like to thank my wife for her patience, love, and support, and my lovely son for adapting to new environments in the USA and Norway.

Nomenclature

ANN	Artificial Neural Network
$B1$	Pitch bending process
$B2$	Yaw bending process
BR	Bayesian Regularization
C	Centroid of a spatial coordinate
CHT	Circle Hough Transform
CL	Clamping process
CMM	Coordinate Measurement Machine
D	Laser moving distance
DS	Data subset
DOF	Degree Of Freedom
FEA	Finite Element Analysis
fps	Frames Per Seconds
G	Segmented image matrix
GA	Genetic Algorithm
gw	Gaussian window
h	Distance from the bend die to the location of interest
H	Desired (die configuration) dimension
H^{md}	Measured dimension
$I(x,y)$	Pixel intensity matrix
IMU	Inertia Measurement Unit
$K(x)$	Gaussian kernel function
L_{fixture}	Fixture span length
$L1$	Straight line at the end of a profile
$L2$	3D curved line
$L3$	2D curved line
$L4$	Straight line at the center of a profile
LASER	Light Amplification by Stimulated Emission of Radiation
LVDT	Linear Variable Differential Transformers

L_i	Length of i^{th} segment
$L_{initial}$	Initial length
$L_{pre\text{-}stretch}$	Pre-stretch length before bending
$L_{ref.}$	Reference length
MPG	Mile Per Gallon
N.A.	Neutral Axis
O_{pitch}	Pivot point for pitch rotation
O_{yaw}	Pivot point for yaw rotation
$P1$	The origin of the local coordinate system
$P2$	Point of intersection between curved lines $L2$ and $L3$
$P3$	Point of intersection between curved lines $L3$ and $L4$
PEEQ	Equivalent plastic strain
R3D4	4-node quadrilateral rigid elements
R_1	Radius in the vertical direction of a bend die
R_2	Radius in the horizontal direction of a bend die
RDB	Rotary Draw Bending
RGB	Red, Green, and Blue
ROI	Region Of Interest
S4R	4-node quadrilateral shell elements with reduced integration
$SC1$	Laser scan process before release
$SC2$	Laser scan process after release
SD	Standard Deviation
ST	Stretch process
κ	Curvature
u	distance between the global and local coordinate systems on the X-axis
v	distance between the global and local coordinate systems on the Y-axis
w	distance between the global and local coordinate systems on the Z-axis
$\Delta\theta$	Springback angle
$\theta_{initial}$	Bending angle before unloading
θ_{final}	Bending angle after unloading
θ_1	Pitch-bending angle before unloading
θ_2	Yaw-bending angle before unloading
θ_I	Initially tilted angle of the rotational joint of the hydraulic actuator

ΔH	Springback dimension
ΔH_1	Springback dimension in the vertical direction of a profile
ΔH_2	Springback dimension in the horizontal direction of a profile
H_1	Desired dimension in the vertical direction of a profile
H_1^{md}	Measured dimension in the vertical direction of a profile
H_2	Desired dimension in the horizontal direction of a profile
H_2^{md}	Measured dimension in the horizontal direction of a profile
ΔL_{pitch}	Moving distance of the motorized actuator
ΔL_{yaw}	Moving distance of the hydraulic actuator

Table of contents

List of figures

Page

List of tables

Page

1. Introduction

1.1. Background

According to dictionary, the definition of *manufacture* is “something made from raw materials by hand or by machinery” or “to make into a product suitable for use” [1]; i.e., manufacturing converts material to useful products. Metal forming is an operation along subtractive and additive processes within the category of manufacturing. It is essentially a manufacturing technique used to shape the material into the desired shape. In the fields of aerospace, architecture, automotive, shipbuilding and others, metal forming plays a significant role in manufacturing (see Figure 1.1).

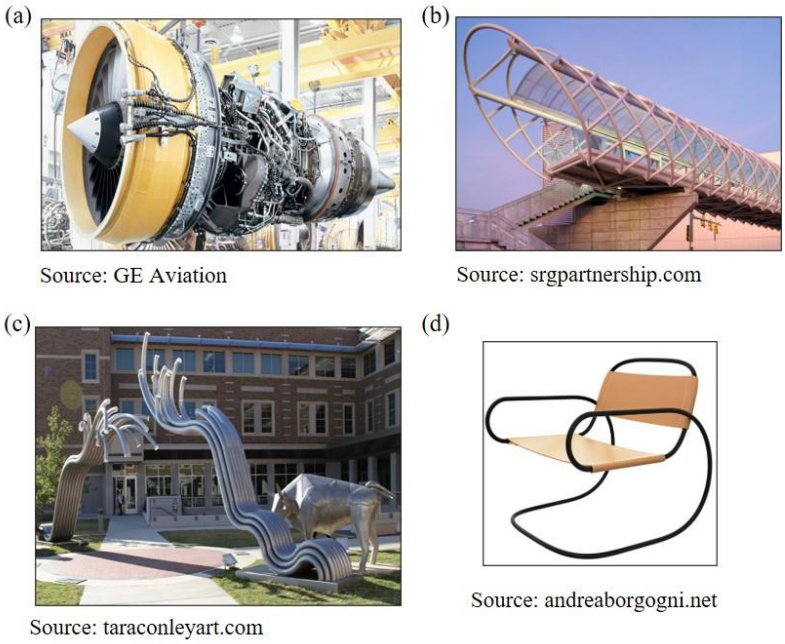

Figure 1.1. Bent products, (a) aerospace; (b) architecture; (c) art; (d) furniture

Although there are many different technologies for producing a product, additional industrial demands such as lightweight, high strength, dimensional accuracy and aesthetics continuously challenge metal forming manufacturers. Hollow structural members for lightweight design or light materials are frequently used to meet industrial demands. In terms of materials, aluminum,

atomic number 13, is the most common metal and the third-most abundant matter in the earth's crust. From a material's point of view, aluminum alloys are of great interest often as a substitute for steel, copper, polymers or other material. Aluminum alloys are highly ductile, making them attractive for e.g. flexible forming. Aluminum alloys, with about a third of the density of steel and a strong affinity for oxygen, are attractive for reducing the weight of a product while providing corrosion resistance in many applications.

Due to the advantages of aluminum alloys, automotive manufacturers use extruded aluminum alloys for crash management systems, such as bumper beams and subframes, to absorb impact energy, see Figure 1.2. Furthermore, automakers employ aluminum extrusions to protect battery packages in electric vehicles as a rapidly growing product. Another example is stiffeners made of aluminum alloys used to reinforce thin-walled structures of aircraft fuselage and wings as well [2].

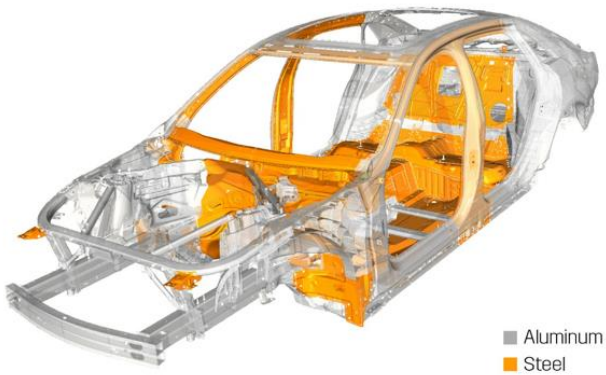

Figure 1.2. Extruded aluminum application to automotive [3]

Various manufacturing industries use aluminum alloys due to their lightweight and mechanical characteristics. Metal forming of aluminum alloy profiles, accordingly, have become increasingly important in manufacturing. Nonetheless, there are different types of quality concerns in metal forming; i.e., springback, wrinkling, tearing, and others. To improve product quality in bending, this research mainly focuses on measuring, prediction, and control of 3D profile bending, with motivation from a desired transition towards the next industrial system 'Industry 4.0' and zero-defect manufacturing.

1.2. Tube bending

Tubular components with curved shapes account for a large portion of finished products in diverse fields, as shown in Figure 1.1 and Figure 1.2. There are various types of manufacturing technologies to make a ‘slanted’ product with a metallic tube; i.e., welding, mechanical joining, and others. Tube bending is one of the most manufacturing processes that satisfy specific curved shapes obtained by bending a material by imposing plastic deformation. In general, a loaded tube in a bending machine is formed by dies or rollers, conforming to the shapes of the tool configuration used. In the process, bending moments are generally applied to form the tube into two or three dimensions.

While tube bending without external forces can be accomplished with, for example, local heating and cooling [4,5], tube bending methods are based on a bend die to apply external forces through movements and contact. Based on tool configurations and kinematics, tube bending methods are divided into compression bending, press bending, roll bending, rotary draw bending, and others.

Figure 1.3 shows compression bending. The basic bending mechanism is straightforward: a tube is fixed to the bend die by the clamp die and the compression die rotates around the fixed tube to directly apply the bending force. During bending, the bend die is stationary. The method provides usually lower quality due to the shear and contact forces. Since an internal mandrel is usually not used in compression bending, the cross-sectional shape can be oval or out of round. Compression bending is less suitable for small-radius bending due to buckling and cross-sectional distortions. Nonetheless, compression bending is a commonly used method in industry due to flexibility, low cost and simple tooling.

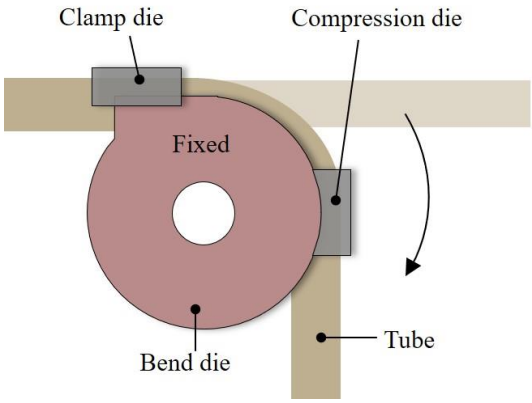

Figure 1.3. Compression bending

Figure 1.4 shows press bending, which is one of the simple bending methods. A tube is supported by two wing dies, and the bending force to the tube is applied by the ram die. An internal mandrel is usually not used in press bending, which sometimes will cause significant cross-sectional deformation. According to [6], it is practical to bend a tube up to maximum165 degrees. This bending method is adequate for thick-walled or large-radius tube bending, and the tooling is relatively inexpensive.

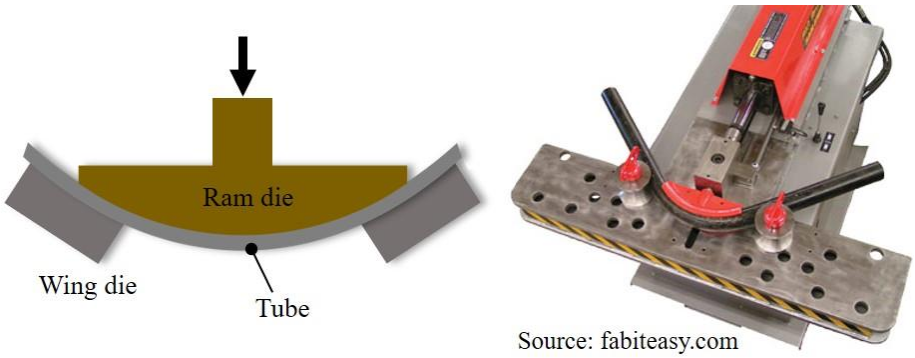

Figure 1.4. Press bending

Rotary draw bending is a popular and commonly used method for tube bending, see Figure 1.5. Rotary draw bending is quite similar to compression bending, but the bend die rotates in rotary draw bending. During the bending process, one of the tube's ends is clamped between the clamp die and the bend die. The pressure die pushes and holds the tube. The bend die, clamp die and tube rotate simultaneously until the desired bending angle is reached. Rotary draw bending

commonly adopts a mandrel inside the tube to prevent local cross-sectional deformations. Not only the circular tubes but also rectangular tubes or channels can successfully be bent in the rotary draw bending. Moreover, rotary draw bending is advantageous in small-radius bending, and multiple bending of a long profile can make two- or three-dimensional part configurations.

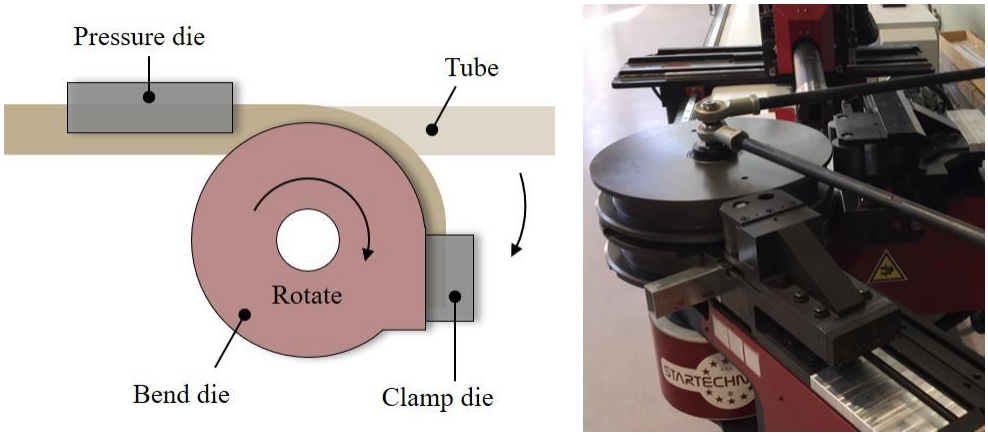

Figure 1.5. Rotary draw bending

In Figure 1.6, roll bending is illustrated. While three rolls are generally used in roll bending, more than three rolls can also be used. As the forming roller moves up or down, the bending radius is determined based on the three contacted points between the tube and rollers. Furthermore, moving the roller during bending can make varying tube curvature along the length as the profile passes through the die assembly. This bending method is flexible and is suitable for large radii. The limitations of roll bending are small radius bending, distortions of thin-walled sections and large elastic springback, and thus variability.

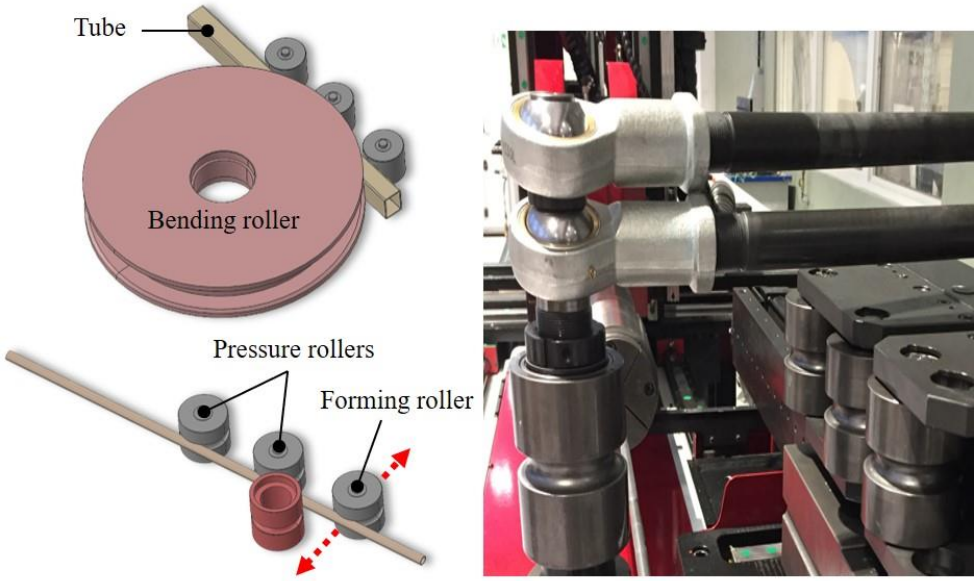

Figure 1.6. Roll bending

In order to reduce deformation after bending, stretch bending methods [7–9] are developed as shown in Figure 1.7. The main concept of stretch bending is to proportionally stretch and bend the tube during the entire forming process. In the figure, the blue-colored arrows indicate the tensile force and the black-colored arrows indicate the bend die movement. The tube is clamped at the ends until forming is finished. Figure 1.7(a) shows so-called force-controlled stretch bending, and Figure 1.7(b) shows so-called strain-controlled stretch bending. While the bend die in Figure 1.7(a) moves transversely, applying a force to bend the tube, the two semidies in Figure 1.7(b) rotate simultaneously. Very low transverse forces, thus, exist in strain-controlled stretch bending due to die rotation. Due to stretching imposing less stress gradients across the cross section, springback in stretch bending is smaller than the other bending methods shown in Figure 1.3 to Figure 1.6.

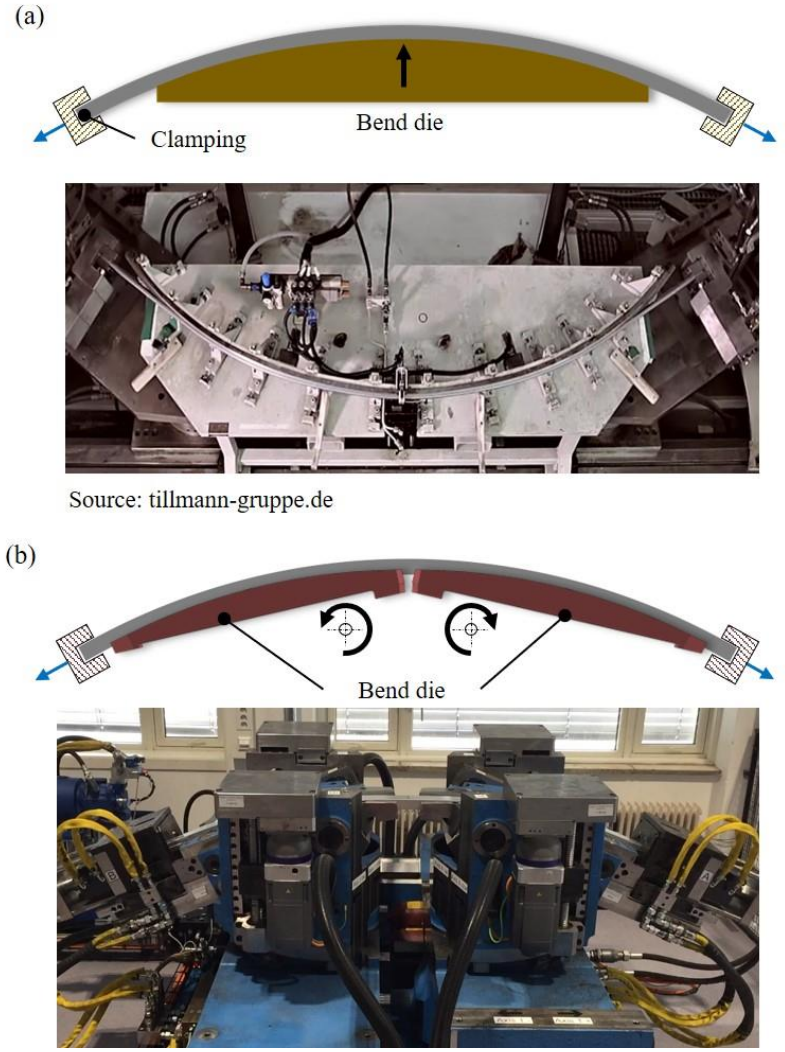

Figure 1.7. Stretch bending, (a) force-controlled; (b) strain-controlled

Nevertheless, several defects such as springback, indentations, local buckling, sagging, etc. may occur, see Figure 1.8. Variations in springback as a global deformation reduce the dimensional quality of the formed product. Although stretch forming in Figure 1.7 can be an option to reduce springback, and thus variability, springback cannot be fully eliminated. Moreover, other defects such as sagging of individual members and other cross-sectional distortion may prevail. Local defects can affect the external appearance of the product and cause the need for a wide

dimensional tolerance of the surface profile. In addition, local deformations affect the stress distribution and may therefore interact with springback.

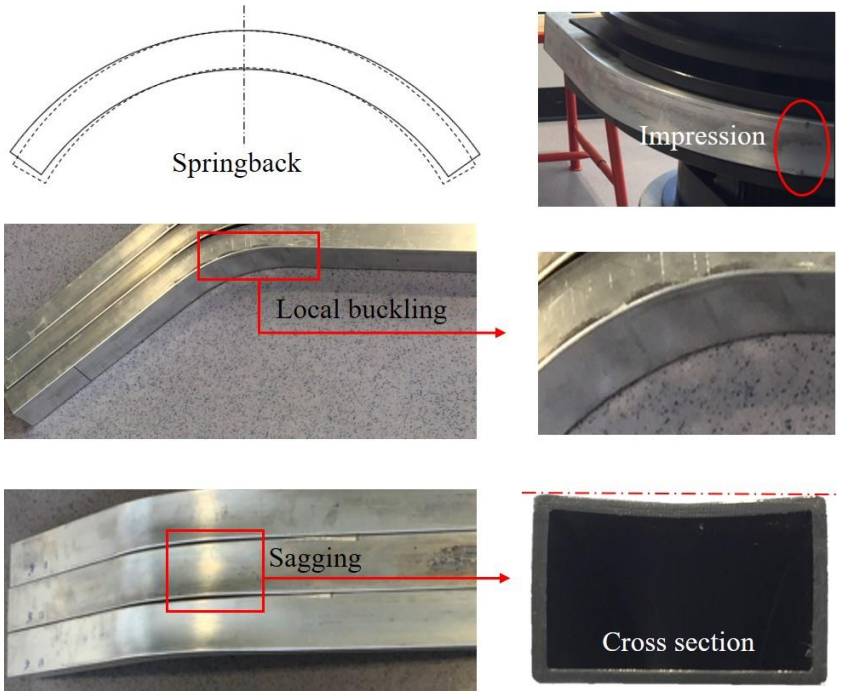

Figure 1.8. Global and local defects in tube bending

Advantages and disadvantages of the above bending methods are compared in Table 1.1. Compression bending is simple for tooling setup, but performance in small-radius bending is limited. While press bending can reduce cycle time and cost, the quality of the bent product may be unacceptable in some cases. Rotary draw bending is popular due to its high accuracy, fast production, repeatability, and others. On the other hand, the setup cost is relatively high. For roll bending, tool change is not necessary for variable curvature bending, but increased flexibility comes with the disadvantage of lower dimensional quality. As mentioned, springback variability is one of the main challenges in tube bending; however, stretch bending can decrease springback and thus reduce variability. Since each bending method has its advantages and disadvantages, a proper bending method should be selected based on the actual product need and manufacturing capabilities in the company.

Table 1.1. Advantages and disadvantages of the tube bending methods

	Advantages	Disadvantages
Compression bending	• Fast production • Simple tooling setup	• Limit of small radius bending • External damage
Press bending	• Fast production • Low tooling cost	• Poor accuracy • Poor repeatability • External damage
Rotary draw bending	• Small radius bending • High accuracy • Fast production • Repeatability	• Expensive setup cost • Tooling dependent bending
Roll bending	• Variable curvature bending • Flexible bending without tooling change	• Limit of small radius bending • Poor accuracy • Poor repeatability • Large springback
Stretch bending	• Less springback • Large part forming	• Complex bending control • Local deformation

1.3. Springback mechanism

When applying an external force to a specimen in a uniaxial tensile test, a typical metallic material such as aluminum experiences deformation, see Figure 1.9. The initial length of the material is continuously stretched until the strain reaches point Y_s. If the final strain is within the elastic region, the imposed deformation of the material recovers to the initial length after unloading. Upon continued deformation beyond the elastic region, the material is plastically deformed. Point Y_s in the plastic region follows the red-colored arrow after unloading, and a permanent deformation remains. The unintended elastic recovery after unloading—springback—depends on the elastic modulus and the stress at the instant of unloading. The higher the elastic modulus E, or the lower the yield strength σ_{yield}, the lower the springback. The plastic strain $\varepsilon_{plastic}$ after unloading can be expressed by

$$\varepsilon_{plastic} = \varepsilon_{total} - \varepsilon_{elastic} \tag{1.1}$$

where ε_{total} is total strain before unloading, and $\varepsilon_{elastic}$ equals σ_{yield} / E.

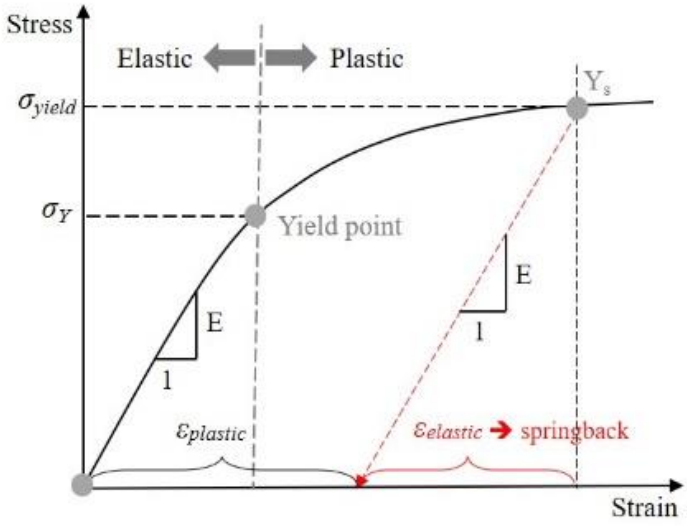

Figure 1.9. Stress-strain relation

Figure 1.10 shows the stress and strain distribution in pure bending. The material in Figure 1.10(a) is approximated with an elastic-perfectly material model. The stress within the elastic region is proportional to the strain with the coefficient of proportionality, and the stress beyond

the elastic limit ② is constant σ_Y .The corresponding beam bending is shown in Figure 1.10(b). It is assumed that the beam deflection follows the classical beam theory due to Euler-Bernoulli. The bending moment is applied to bend the beam; the initial bending angle is $\theta_{initial}$; the bending radius is $\rho_{initial}$. Upon bending the extrados of the beam is stretched; the intrados is compressed. The neutral axis denoted by *N.A.* is a layer with zero strain or stress, which is indicated by the dotted line at the beam center, assuming a symmetrical cross section and a material that behaves equally in compression and tension. The strain distribution and the stress distribution under bending are shown in Figure 1.10(c) and (d). The blue color in the stress distribution indicates tensile stress, and the orange color indicates compressive stress. When the extrados and intrados are still in the elastic region, the stress in the y-direction is linearly distributed across the depth of the cross section. The assumption is that the cross section is symmetric. Thus, the bending stress at mid height of the cross section (the neutral axis) is zero. In this case, the final bent angle becomes zero after unloading due to purely elastic deformations. As the bending angle increases, the strain in the vicinity of the extrados and intrados get deformed into the plastic region. When the total strain in the y-direction is within the plastic region, the magnitude of the tensile and compressive stress is σ_Y . After unloading, the final bent angle generally becomes smaller than the initial bending angle.

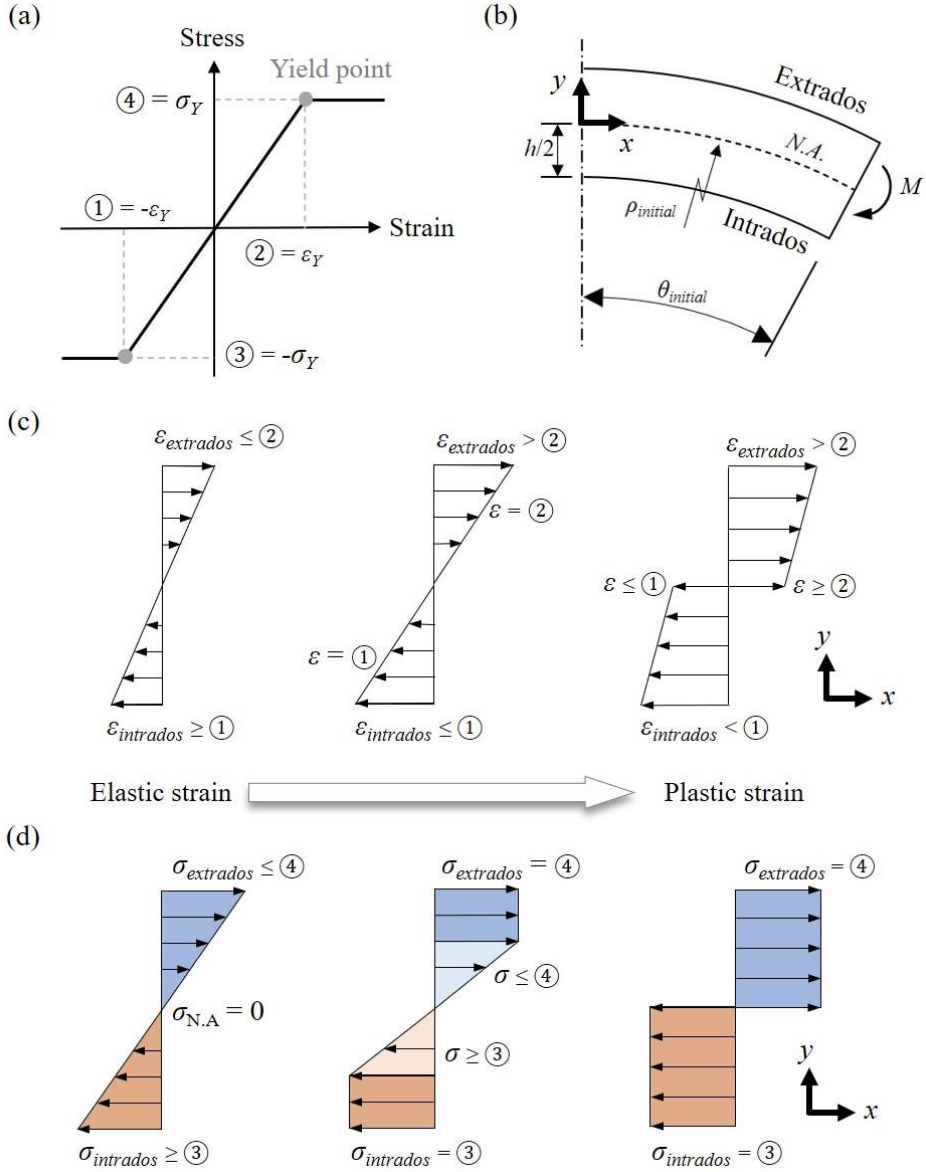

Figure 1.10. Bending; (a) elastic-perfectly plastic material; (b) pure bending; (c) strain distribution; (d) stress distribution

Figure 1.11 illustrates the bent shape of a solid rectangular beam before unloading and the final shape after unloading. The dark and light gray colors indicate the bent and final shapes,

respectively. After springback, the final bending radius ρ_{final} is larger than the initial bending radius $\rho_{initial}$.

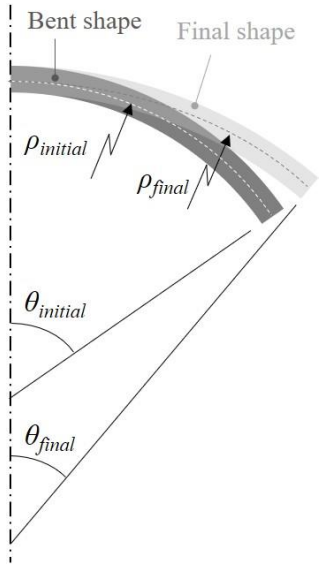

Figure 1.11. Shapes before and after springback

From geometry, the arc length of the neutral axis *N.A.* before springback and after springback does not vary, which be expressed as,

$$\rho_{initial}\theta_{initial} = \rho_{final}\theta_{final} \tag{1.2}$$

While the arc length of the neutral axis does not change, the initial bending radius $\rho_{initial}$ is changed due to springback. The springback angle $\Delta\theta_{spb}$ is the difference between the initial bending angle $\theta_{initial}$ and the final bending angle θ_{final}. This change in springback angle can be expressed by

$$\Delta\theta_{spb} = \theta_{initial}(1-\frac{\theta_{final}}{\theta_{initial}}) \tag{1.3}$$

The curvature $\kappa(=1/\rho$ for small deformation) is changed, and the change of the curvature $\Delta\kappa$ can be expressed by

$$\Delta\kappa = \frac{1}{\rho_{initial}} - \frac{1}{\rho_{final}} \tag{1.4}$$

This curvature change $\Delta\kappa$ is a characteristic that indicates the magnitude of springback locally. Assuming constant bending along the segment, the springback angle $\Delta\theta_{spb}$ is given by

$$\Delta\theta_{spb} = \rho_{initial}\theta_{initial}\Delta\kappa \tag{1.5}$$

In industrial practice, there are many factors that affect springback in bending— bending speed, friction, temperature, material properties, and others, the cross-section of the beam and the bending moment are only considered to calculate springback. The bending moment M from the stress distribution in Figure 1.10(c) can be calculated by

$$M = \int_{-h/2}^{h/2} \sigma_Y b_w y dy \tag{1.6}$$

where b_w and h are the width and the depth of the cross section, respectively. It presumes that elastic stresses are not neglected. The bending moment M is simplified as following

$$M = \frac{\sigma_Y b_w h^2}{4} \tag{1.7}$$

Figure 1.12 is the moment-curvature curve of the beam. After unloading, the point P_{final} moves to the point P_{pl} along the red-dotted arrow.

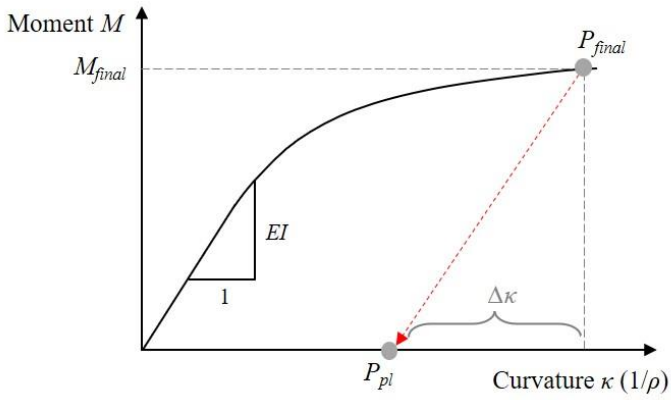

Figure 1.12. Moment-curvature curve

With the change of the curvature $\Delta\kappa$, the springback angle $\Delta\theta_{spb}$ is calculated as follows

$$\Delta\theta_{spb} = \rho_{initial}\frac{3\sigma_Y}{Eh}\theta_{initial} \tag{1.8}$$

It is shown that the material properties and the depth of the cross-section based on Eq. (1.8) affect the springback angle. Higher strength σ_Y causes larger springback; higher elastic modulus E and depth h both reduce springback.

1.4. Springback compensation and control

In metal forming, including tube bending, the ultimate goal is to make a product whose geometry is within the dimensional tolerances of the nominal shape. To meet the dimensional quality requirements, various approaches, such as feedback control, overbending, or tool shape adjustment are used to compensate for or control springback. Given that springback cannot be accurately eliminated due to variations in material properties, springback variability after bending can be controlled with several approaches [10]: (i) load-unload (prediction of next stop position)-load-unload, (ii) iteration of load-unload, and (iii) one-hit bending with sensor data and a physical model. Trial-and-error is also a commonly used strategy for springback compensation. This experience-based compensation, however, requires multiple attempts—iterative processing—and is not adequate for manufacturers who consider tooling design time and cost saving.

A re-bending strategy is one of the springback compensation methods that uses multiple bending. This approach requires multiple trials until the springback angle reaches the target angle. In addition, springback can be compensated by adjusting the shape of the bend die. According to [11], the traction field to achieve the desired shape can play a role as an indicator for the final die shape and springback compensation. When the traction field $\mathbf{f}^i$ in the i^{th} iteration is the same as the traction field $\mathbf{f}^{i+1}$ in the $(i+1)^{\text{th}}$ iteration, the displacement field of the bent shape $\mathbf{u}_{ul}^i$ is the final die shape as indicated in Eq. (1.9). These re-bending steps help to find the die shape for springback compensation.

$$\mathbf{u}_{ul}^i = \mathbf{u}^* - \mathbf{u}_{spb}^i(\mathbf{f}^i) \tag{1.9}$$

Another tooling design method for springback compensation is the displacement adjustment (DA) method developed by Gan and Wagoner [12]. After springback, the die shape and bent shape are compared, and the shape error is defined. To compensate springback, the die shape in each iteration is modified as much as the shape error until the bent shape falls within the tolerance band of the product. The DA method is a non-theoretical based approach, which is given by

$$\mathbf{X}_{tool}^{i+1} = \mathbf{X}_{tool}^i + \Delta\mathbf{y}^i \tag{1.10}$$

where $\mathbf{X}_{tool}^{i+1}$ and $\mathbf{X}_{tool}^{i}$ indicate the die shape before and after shape adjustment, respectively, and $\Delta\mathbf{y}^{i}$ is the shape error. According to [13], the 3D shape deviations between the die and the bent product can be efficiently measured by 3D scanning instead of traditional measurement fixture. Using the deviation data, the die surface is adapted to springback compensation.

Another method is to correct bending processes for variations. Figure 1.13 shows block diagrams of open and closed-loop control systems. The difference between the two control systems is the presence of a feedback process in the control system. The open-loop system uses input data only once and delivers outputs, which is more applicable to mass production due to its non-iterative process scheme. It is a simple and inexpensive method for springback compensation. Thus, manufacturers can reduce product lead time and save manufacturing costs. On the other hand, the springback compensation algorithm in the open-loop system must be accurate because machine setting can be determined by the algorithm.

The closed-loop system for feedback control aims to control the process within one cycle. Based on the input parameters (machine inputs), the output values are compared with the target angle. In order to achieve the desired specification, updated inputs are feedbacked to the bending machine. The in-line measurement or sensing technology is important to provide feedback. Using the sensing data, this bending strategy is implemented until the specified criteria are satisfied. The iterative feedback process can increase cycle time to compensate springback compared to the open-loop system.

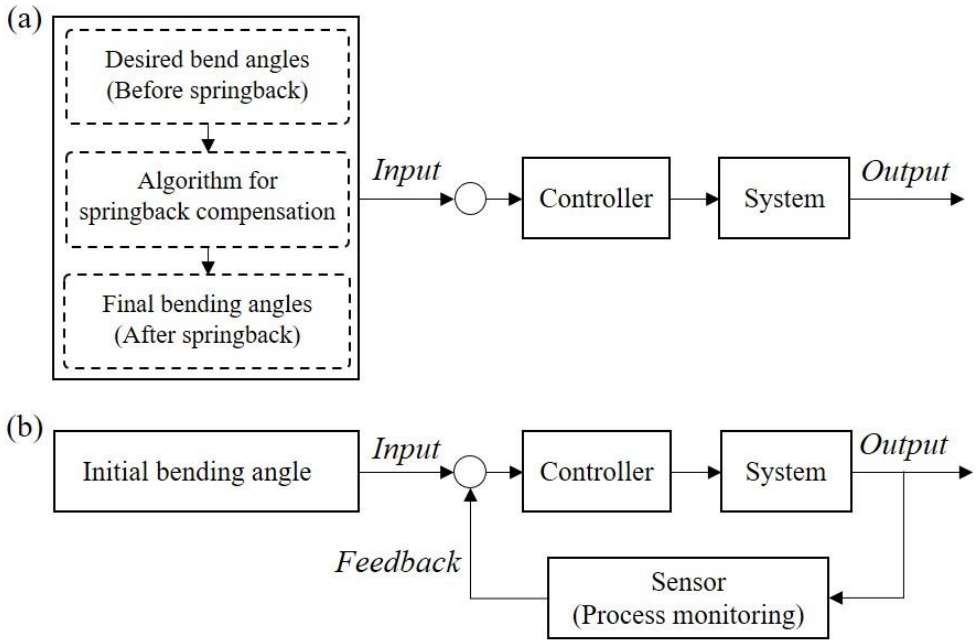

Figure 1.13. Block diagram for springback control, (a) open-loop system; (b) closed-loop system

1.5. Artificial neural network

Artificial neural network (ANN) is extensively used to analyze complex data or predict a tendency without theoretical modeling. For tube bending, ANN can be employed to predict or control springback. ANN, also known as neural network (NN), is one of the calculation algorithms, reflecting the nervous system of humans. Figure 1.14 shows the overall architecture of artificial intelligence (AI). ANN is a branch of machine learning (ML) and a fundamental algorithm for deep learning (DL). In the 1950s, Rosenblatt [14] developed the simplest neural network, called a perceptron. The perceptron, a classification algorithm, makes output by weighting input data. While the initial perceptron, which is a single layer, classifies linear logic gates—AND, OR, and NOT, it is limited by its inability to classify a non-linear logic gate such as XOR. To overcome the non-linear problem, multilayers are introduced. Currently, various ANNs including convolutional neural network (CNN), recurrent neural network (RNN), and support vector machine (SVM) are used for computer vision, pattern recognition, regression, natural language processing, and others.

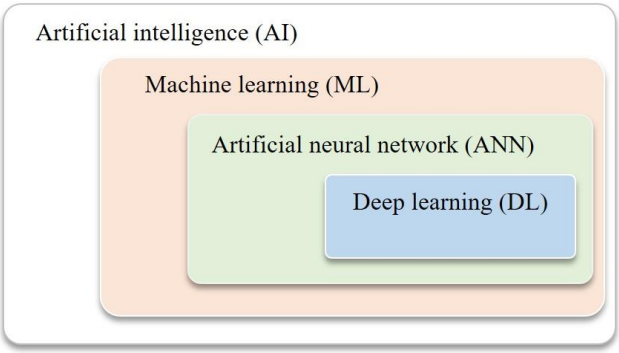

Figure 1.14. From artificial intelligence to deep learning: architecture

Figure 1.15(a) illustrates an artificial neural network. ANN simulates biological nervous mechanisms [15]. In the human nervous system, each end of the neuron is interconnected to other neurons, which is the pathway for communication. ANN comprises three layers: input, hidden, and output layers. Each layer has nodes corresponding to neurons and connected to other nodes. A weight between two nodes is used to scale the output values for signal propagation. Outputs are obtained by weighting nodes' values from the input layer via hidden

layers. This type of ANNs is a feed-forward neural network, which is trained by back-propagation. The back-propagation is repeated until the optimal weights are obtained.

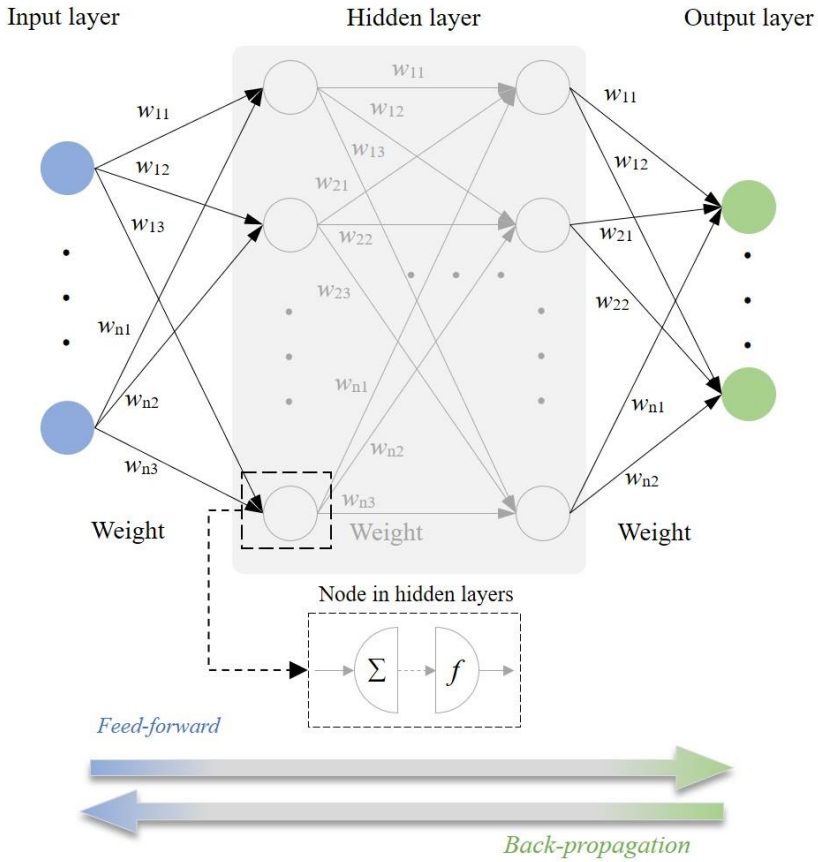

Figure 1.15. Schematic diagrams of an artificial neural network

The summation of the input values is converted into the output value through nonlinearity *f*, called an activation function. The classical linear and non-liner activation functions are listed in Table 1.2.

Table 1.2. Activation functions in artificial neural networks

Function	Formula	Remarks
Identity	$f(x) = x$	Linear
Hyperbolic tangent	$f(x) = \frac{(e^{x} - e^{-x})}{(e^{x} + e^{-x})}$	Non-linear
Arc Tangent	$f(x) = \frac{2}{1 + e^{-2x}} - 1$	Non-linear
ReLU	$f(x) = \max(0, x)$	Non-linear
Logistic	$f(x) = \frac{1}{1 + e^{-x}}$	Non-linear

The computed outputs are obtained by weights and activation functions based on given inputs. Differences between the outputs and computed outputs are quantifiable. The loss function *L* evaluates the learning performance. There are several types of loss functions in regression as listed in Table 1.3. For linear regression, square loss and absolute loss are the most common loss functions. While the square loss function is very sensitive to outlier data due to the square of the error, the absolute loss function is less sensitive to outliers. The goal in ANN is to minimize loss and to iterate towards optimal weights by finding minimal optimum (see Figure 1.16).

Table 1.3. Loss functions [16]

Function	Formula	Algorithm
Square loss	$L(y, f(x)) = (y - f(x))^2$	Linear regression
Absolute loss	$L(y, f(x)) = \lvert y - f(x) \rvert$	Linear regression
Log-cosh loss	$L(y, f(x)) = \log(\cosh(f(x) - y))$	Extreme gradient boosting
Quantile loss	$L_{\gamma}(y, f(x)) = \begin{cases} (\gamma - 1)(y - f(x)), & \text{if } y < f(x) \\ \gamma(y - f(x)), & \text{if } y \geq f(x) \end{cases}$ *where* $\gamma \in (0,1)$ is given quantile	Quantile regression

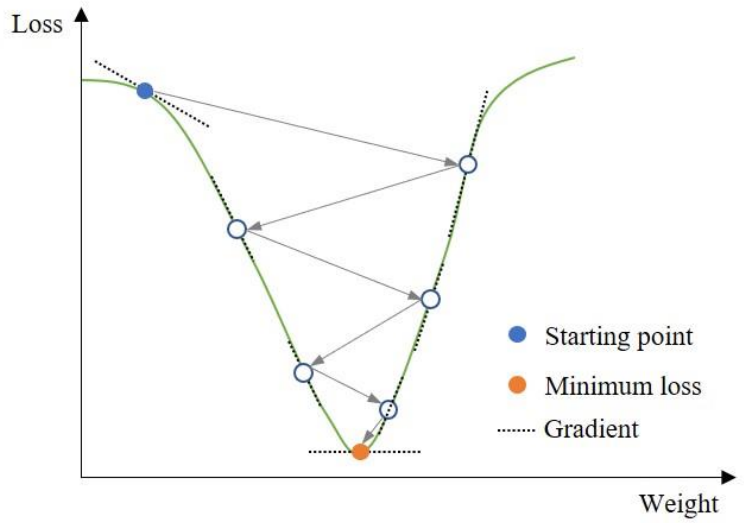

Figure 1.16. Loss function optimization

ANN is sometimes referred to as a black box, and is a sort of established correlation between given input and output data. When conducting ANN analysis, the sample size is important. Although there are not exact rules to determine the sample size, there are rules-of-thumb [17]; i.e., (50~1000) × the number of output classes, (10~100) × the number of features and 10 × the number of weights. If high quality and sufficient amounts of data sets including complex and non-linear data for training ANN are provided, ANN can produce a non-linear prediction model and solve complex problems. Thus, ANN can apply to various fields. ANN was used for establishing a cost prediction model in pipe bending [18]. Haghdadi et al. [19] analyzed the flow behavior of a cast aluminum alloy under 400~540 ºC with ANN, and Hsiang et al. [20] investigated thermo-mechanical properties of hot extruded magnesium alloy under 320~400 ºC. The ultimate bending moment of steel tubes in pure bending [21] and the flexural overstrength factor (local buckling load vs. yield stress) of structural steel pipes [22] were predicted by ANN. By controlling forming parameters predicted by ANN, springback variations due to variations in material properties and frictional conditions in channel forming were minimized [23]. For improved product quality and manufacturing speed, a combination strategy of ANN and fundamentals of plasticity theory was used to control the variable blank holding force in deep drawing [24]. To obtain optimal bending parameters in L-bending, ANN was employed to provide data sets for the optimization algorithm [25]. Furthermore, Ma et al. [26] used ANN for springback prediction and compensation in rotary draw bending, and improved the

geometrical quality of the bent tube by the bending angles predicted by ANN. ANN is a data-driven based approach without explaining physical manufacturing phenomena. Therefore, ANN is believed to be a useful method to predict product quality and improve manufacturing processes towards Industry 4.0.

1.6. Research statement

1.6.1. Research problems

Most bending methods cause plastic deformation, producing permanent deformation and thus a shape different from the original one. Since the cross section of a straight aluminum profile is efficiently formed in extrusion, profile bending can be an ideal process for providing a curved configuration of the extrusion. Moreover, bending is a method used for reducing weight by part consolidation and need for joining interfaces. However, springback variations can cause a quality problem for the finished product.

Springback in profile bending can be predicted by theoretical modeling or numerical simulation. The theoretical approach may help efficiently predict springback after bending, and numerical simulation can provide accurate information regarding stress or strain distribution during and after bending. Nonetheless, accurate springback prediction is difficult due to the complexity associated with material product and process interactions. In addition, the geometrical complexity in 3D bending also hinders springback prediction.

In order to check geometrical quality, the geometric dimensions of the finished product are measured after completing the forming process. Springback measuring methods using a length gauge, a radius gauge, or an angle gauge are capable of obtaining off-line measurement data. The off-line measurement methods, however, are limiting in monitoring springback in real time or measuring springback on the machine.

Digital data acquisition and analysis during bending processes are required for Industry 4.0. In Industry 4.0, the integrated sensing systems in the manufacturing machines are essential for real-time monitoring, aiming to achieve the smart factory by the cyber-physical system (CPS) technology [27]. Real-time data including process monitoring, springback measuring, and others, should be acquired to achieve digital manufacturing.

1.6.2. Research objectives

Figure 1.17 illustrates extrusion-making in upstream processes. Material and geometric properties, and their variations, are created in upstream processes prior to the forming step. Semi-finished tubes in batches are delivered from aluminum extruders. Thus, the final product quality and manufacturing processes are significantly influenced by upstream processes.

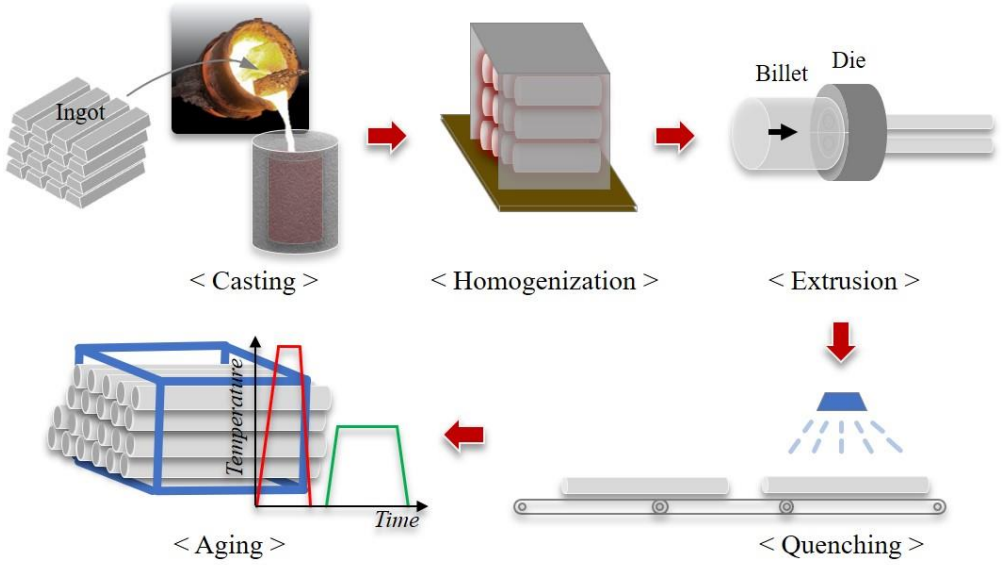

Figure 1.17. Illustration of the upstream processes for extrusion

The primary objectives of this dissertation are to measure and monitor springback in real-time, and to predict and control springback in order to improve the dimensional accuracy of 2D and 3D profiles bent in stretch bending. As shown in Figure 1.18, the main objectives are deduced with respect to manufacturing processes towards Industry. 4.0. In order to accomplish the research objectives, the following tasks are conducted:

- Task 1: suggest non-contact measurement methods to capture the deformation of a profile.
- Task 2: evaluate the possibility of the digital-image based on-machine measurement.
- Task 3: develop a kinematic analysis to identify the 3D shape of a profile.
- Task 4: identify the mechanical relations between actuator operations and bending angles.
- Task 5: develop a model to predict 2D and 3D springback.

- Task 6: investigate the effect of stretch before bending in 2D and 3D stretch bending.
- Task 7: propose an ANN model to control springback and use the model to save experimental costs.

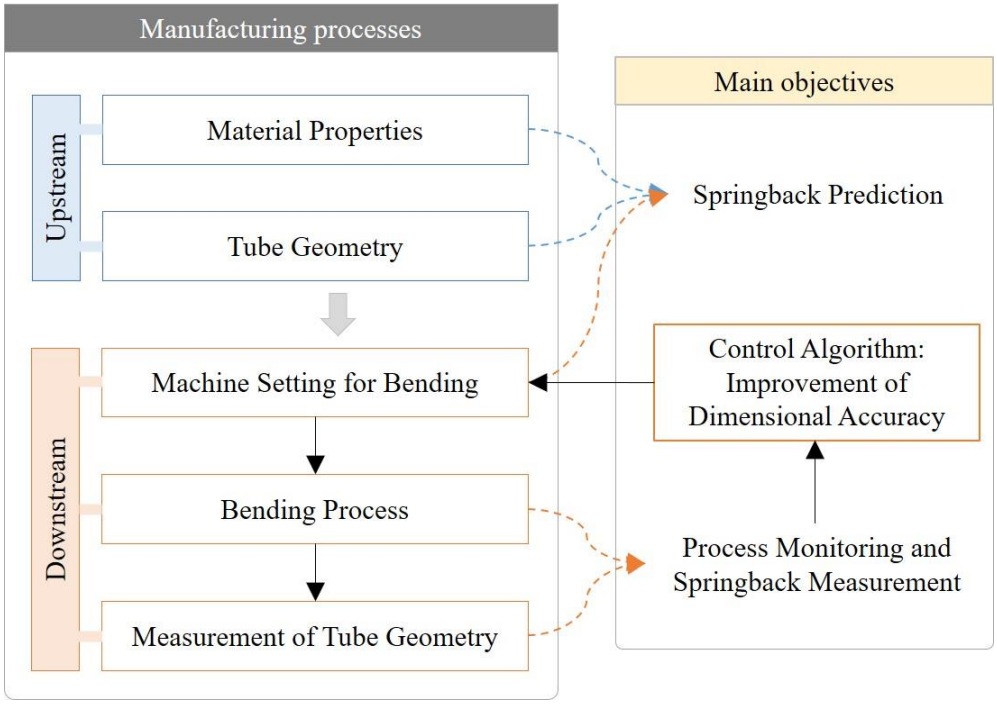

Figure 1.18. Main objectives

1.6.3. Papers for dissertation

This doctoral thesis comprises published/submitted journal papers and one conference paper which are produced during the Ph.D. study. Figure 1.19 presents the relation between research objectives and papers. Seven tasks are linked to three main objectives, and those seven tasks are discussed in four papers. The papers written to accomplish the main objectives are presented in this doctoral dissertation. Paper I covers springback measurement and monitoring in rotary draw bending. The fundamental measurement approach is connected to paper II, which is related to stretch bending. Papers II, III, and IV cover the overall main objectives in 2D and 3D stretch bending.

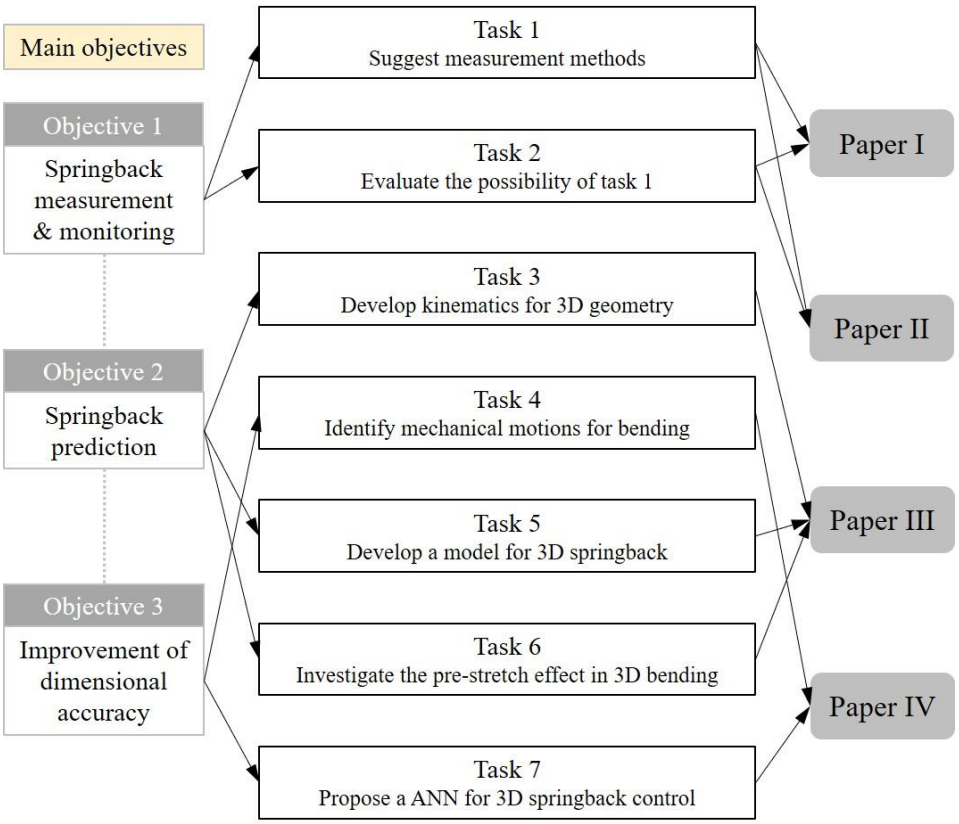

Figure 1.19. Relation between research objectives and papers

A brief overview of each paper is provided as follows:

Paper I (Journal paper)

'A strategy for on-machine springback measurement in rotary draw bending using digital image-based laser tracking'

- Authors:Taekwang Ha, Torgeir Welo, Geir Ringen, Jyhwen Wang
- Status: published in International Journal of Advanced Manufacturing Technology 119 (2022) 705–718, DOI: 10.1007/s00170-021-08178-w
- Research objective: measure and monitor springback in real time.
- Brief description:

  A cost-effective system for on-machine measurement is used to measure springback in rotary draw bending with an affordable 635 nm laser and a webcam. A target board displays a laser beam installed at the end of a profile. The web cam acquires the target board images in real time. By extracting the laser beam from the acquired images, the location of the laser beam is identified and monitored. The springback angle, then, is evaluated with the actual travel distance of the laser beam on the machine.
- Contribution of the paper:

  An image processing technology is integrated with the manufacturing process to track the deformation and measure the springback angle in real time. The measurement strategy with the integration of a laser and an image processing technology enables springback angles to be measured on a machine and a bending process to be monitored in real time. The method eliminates the need for the workpiece to be transferred to a measurement device. On-machine measurement using laser tacking, thus, can be used as a springback measurement technique for Industry 4.0.
- Personal contribution:

  First author; led the writing of the original draft and finalized the article with feedback from co-authors. Proposed a measurement methodology. Developed the software code for computer-vision based laser tracking. Conducted sample preparation and all experiments. Analyzed experimental results. Prepared all figures.

Paper II (Peer-reviewed conference paper)

'A computer vision-based, in-situ springback monitoring technique for bending of large profiles'

- Authors: Taekwang Ha, Jun Ma, Jørgen Blindheim, Torgeir Welo, Geir Ringen, Jyhwen Wang

- Status: presented in 24th International Conference on Material Forming—ESAFORM 2021, Liège, Belgique, DOI: 10.25518/esaform21.4002
- Research objective: measure and monitor springback in real time.
- Brief description:

  The three reference points on a profile in stretch bending are used to track the deformation of the workpiece with image processing. The reference points marked on the profile's side are partially hidden and incomplete circles. Those points are detected by locally setting regions and filtered to extract the point's center from the complex background. Using the center of each point, springback is evaluated by tracking the position change of the points.
- Contribution of the paper:

  While general measurement tools and machines are available to measure springback, they cannot easily accommodate large products due to the size limit of measurement devices. This paper provides an in-situ springback monitoring technique for bending large-size profiles due to the measurement restrictions for such profiles. Springback in stretch bending can be evaluated based on the computer vision technique. The circular hough transform (CHT) algorithm enables the identification of the center of the hidden and incomplete reference points. As a sensor-based springback monitoring system, this measurement strategy helps to evaluate springback without taking the workpiece from the machine and can be applied to control product quality and move towards Industry 4.0.
- Personal contribution:

  First author; led the writing of the original draft and finalized the article with feedback from co-authors. Proposed a measurement methodology. Developed the software code for image processing. Conducted experiments with the help of co-authors. Analyzed experimental results. Prepared all figures.

Paper III (Journal paper)

'On kinematics in sequential three-dimensional (3D) stretch bending: analytical springback model'

- Authors: Taekwang Ha, Torgeir Welo, Geir Ringen, Jyhwen Wang
- Status: submitted to Journal of Manufacturing Science and Engineering

- Research objective: predict springback in 3D stretch bending
- Brief description:

  The 3D bending geometry is calculated from the homogeneous transformation of the rotated bend die. The variable-curvature 3D bend geometry is discretized and expressed by the Frenet-Serret theorem, enabling the geometry to be described with tangent, normal, and binormal vectors. Integrating all discretized segments, the global springback after unloading is efficiently predicted. This generalized analytic approach and numerical simulation are applied to evaluate springback in both 2D and 3D stretch bending of a thin-walled aluminum profile with a rectangular cross-section.
- Contribution of the paper:

  This work gives a springback prediction method for varying curvature 3D profile/tube bending. A kinematic model for 3D stretch bending is established from the rotational motion of the bend die. The discretized curvature of a bent profile geometry is described by using the Frenet-Serret frames, and a model for springback prediction is further developed based on the kinematics analysis of the bending process. This developed model is able to evaluate the 3D springback of a profile with arbitrary cross-section efficiently for product design and development.
- Personal contribution:

  First author; led the writing of the original draft and finalized the article with feedback from co-authors. Developed the kinematic model for 3D bending. Conducted experiments and numerical simulation. Analyzed analytic, numerical, and experimental results. Prepared all figures.

Paper IV (Journal paper)

'Smart control of springback in advanced stretch bending by an artificial neural network'

- Authors: Taekwang Ha, Torgeir Welo, Geir Ringen, Jyhwen Wang
- Status: submitted to Journal of Manufacturing Processes
- Research objective: improve dimensional accuracy
- Brief description:

  For a complex and non-linear springback problem, an artificial neural network (ANN) as a data-driven approach is an attractive option to establish a springback prediction or control model. The ANN is trained with a small number of experiments and

supplementary analytical data sets. The trained ANN is validated with experiments, showing that springback in 2D and 3D stretch bending can be controlled by the bending angles from the ANN prediction.

- Contribution of the paper:

  This paper presents an efficient method to control springback by an ANN and to improve geometrical quality in 2D and 3D stretch bending. The method utilizes a small number of experiments for ANN training by adopting supplementary data sets from an analytical springback model. The ANN provides adjusted bending angles for springback control. This approach for springback control can be applied to obtain the desired geometry and improve geometrical quality without a large number of experiments.

- Personal contribution:

  First author; led the writing of the original draft and finalized the article with feedback from co-authors. Designed the experimental study with the help of co-authors. Developed the ANN model for springback control. Conducted experiments and analyzed results. Prepared all figures.

1.6.4. Dissertation outline

As mentioned, the dissertation consists of three (targeted) journal papers and one conference paper. The two papers in Chapters 2 and 3 are published in an international journal and presented at an international conference, respectively. The two papers in Chapters 4 and Chapter 5 are submitted to international journals.

The remainder of the dissertation outline is as follows.

- Chapter 2 introduces a digital-image based on-machine measurement strategy in rotary draw bending. The on-machine sensing technology is developed to capture the deformation of a profile using laser image tracking, enabling non-contact measurement. (Paper I)
- Chapter 3 presents an in-situ springback measurement strategy based on image processing in stretch bending. Instead of laser tracking, reference points on the profile are used for springback measurement. (Paper II)
- Chapter 4 demonstrates the kinematics of the semi-die motions and an analytical springback model for 3D stretch bending. Using the kinematic analysis, the allowable yaw bending limit with respect to the pitch bending angle is formulated. (Paper III)
- Chapter 5 demonstrates springback control of a profile with an ANN for 2D and 3D stretch bending. The ANN trained with experimental and analytical data is used to adjust bending angles for springback control. (Paper IV)
- Chapter 6 provides the overall summary of the dissertation and future work for advanced stretch bending.

2. A strategy for on-machine springback measurement in rotary draw bending using digital image-based laser tracking*

2.1. Introduction

The constant striving for cost reduction, quality improvement, and lightweighting of products is a significant challenge to many manufacturing industries. This leads to the preference for relatively light-weight materials, but controlling springback after forming presents a challenge for processing-sensitive lightweight alloys. As a countermeasure, springback, due to elastic recovery after unloading in a metal forming process, is controlled by a feedback control algorithm to satisfy the required final geometric dimensions [28]. Welo and Granly [10] used an analytical model for feedback control of a rotary compression bending. The closed loop model was operated in real time, and the torque and the rotation angle were measured in-process for feedback control. Löbbe et al. [29] controlled springback in progressive bending with induction heating. The induction heating was controlled by a feedback algorithm through measured a springback angle. According to Pan and Stelson [30], the optimal process for springback compensation is traditionally achieved by the less scientific approaches, i.e. operator's experience, skill, or trial-and-error. Multiple bend trials are essential, which finds a better bending process. Borchmann et al. [31] demonstrated that by conducting a sensitivity analysis of practical bending tests and developing a digital equipping support database the product quality could be made user-independent. Since springback control or compensation begins with knowing the status of product's geometry regardless of automatic control or manual control, the first step to control the product quality is to acquire an accurate dimensional change due to springback.

Geometric measurement is fundamental to assess product dimensions, monitor manufacturing processes, and improve product quality. To monitor and evaluate springback in a bending process, different types of measuring techniques have been developed based on contact or non-contact methods. Since a bevel protractor is simple and relatively less time-consuming to measure an inner or outer angle, it is often used to measure springback angles: springback

* Reprinted with permission from T. Ha, T. Welo, G. Ringen, J. Wang, A strategy for on-machine springback measurement in rotary draw bending using digital image-based laser tracking, Int. J. Adv. Manuf. Technol. 119 (2022) 705–718

relationships between parameters influencing springback [32], validation of a feedback system for springback compensation in air bending [33], springback evaluation of sheet metals in vee bending using a neural network [34], and so on. While a bevel protractor can be a good approach to measure an angle between flat surfaces, in the case of a tube or a rounded product, it is sometimes challenging to align the tangential surfaces with a protractor. A coordinate measurement machine (CMM) is also commonly used to accurately measure geometry dimensions by physically touching measuring points, but being less efficient to acquire the data on the grounds that the bent samples are transferred to a CMM and collecting many sampling data takes much of measuring time. Wang et al. [33] adopted linear variable differential transformers (LVDT) to calculate bending angles of loading and unloading cycles in air bending. The measured values were used for feedback control in incremental air bending. Ghiotti et al. [35] presented an in-line measurement method for real-time springback measurement by embedding an inertia measurement unit (IMU) into a mandrel in three-roll bending. The IMU attached to the mandrel allows the springback to be measured in a single process, but the use of the springback measurement method presumes the existence of a mandrel. A closed-loop controlled profile bending platform developed by Welo and Granly [10] recorded in-process torque and rotation to indirectly measure springback. The closed loop feedback control showed three times more process capability of dimension than traditional processes. Although the parameters such as torque and rotation are measured in the process, the accuracy of the springback measurement depends on the accurate prediction model to calculate springback using a steering model with directly measured parameters as input.

With the latest advancement in image processing or computer vision technology, new approaches integrating optical technologies for springback measurement have been applied to metal forming. Wang et al. [13] compared the geometry model to a rebuilt configuration of an automotive panel by scanning point data on the panel surface. The obtained data were used to update the die for springback compensation. Katona et al. [36] integrated three-dimensional optical measurement to inspect a bent pipe in a pipe bending process, as an alternative to a conventional inspection gauge. An optics-aided measurement helps save processing time for quality control, as well as evaluate the product status without removing the workpiece in process. A laser is frequently used as reference to mark targets for measuring distance or position in real time [37] due to its outstanding characteristic of the so-called laser directionality, which is a non-contact measurement technique applicable of springback measurement. Ha et al. [38] measured springback angle on the tube bending process by

installing a laser fitment at the tip of a circular tube and capturing the laser moving distance on the target board. One of the limitations of the measurement method is that the laser moving distance needs to be manually read, and this is time consuming and causes time-delay when evaluating springback angle. Löbbe et al. [29] employed two parallel laser sensors to measure springback angle at different temperatures of progressive die bending. The laser sensors installed in the die gauged the distance to the workpiece, and the bent angle was calculated with the triangulation principle. The measurement technique demonstrated a capability of ±0.25° measurement error. The applicability of laser sensors relies upon sufficient space to install them on a die, though.

Many springback measurement techniques have strong capabilities in obtaining accurate measurement data. Sensor based in-line measurement, however, can facilitate the adoption of Industry 4.0. In-line measurement techniques allow real time monitoring of manufacturing processes. By identifying the current status of tube bending, for example, the monitoring system can be connected to a control system to adjust the process parameters to meet product quality requirement. To replace an off-line quality control and expensive inspection procedures, this paper addresses an easily manageable, simple, and cost-effective on-machine measurement technique to monitor springback in rotary draw bending (RDB) in real time, by integrating image processing based laser beam tracking. It allows springback angle in RDB to be conveniently measured by an affordable sensing system.

The goal of this research is to develop a new strategy for on-machine springback measurement focused on RDB. The measurement strategy and the laser tracking technique using digital images are addressed in Section 2.2. In the present study, a 635 nm laser installed at the tip of a profile was tracked to observe the profile's elastic behavior in different bending cases. An image processing technology using a MATLAB platform was integrated for data acquisition during the bending process in real time. Presented in Section 2.3, image enhancement techniques [39], i.e. image quantization, binarization, and segmentation, were applied to make input images suitable for laser beam tracking. Section 2.4 shows the on-machine measurement experiments and the comparison between the measurements from the proposed method and the conventional manual method. Conclusions of the present research are presented in Section 2.5.

2.2. Proposed Springback Measurement Concept

Previously, Ha et al. [38] suggested an in-line springback measurement method by installing a laser fitment at the tip of a profile and manually reading the laser travel distance on a graph paper attached to a datum board, as shown in Figure 2.1. Geometric deformation of a profile is shown as laser moving on the target. Although the method is appropriate to measure in-line springback angle, it takes time to manually read the laser moving distance based on the grid size. Figure 2.1 illustrates an experimental system for in-line springback measurement and the laser beam spot of loading and unloading on the datum board.

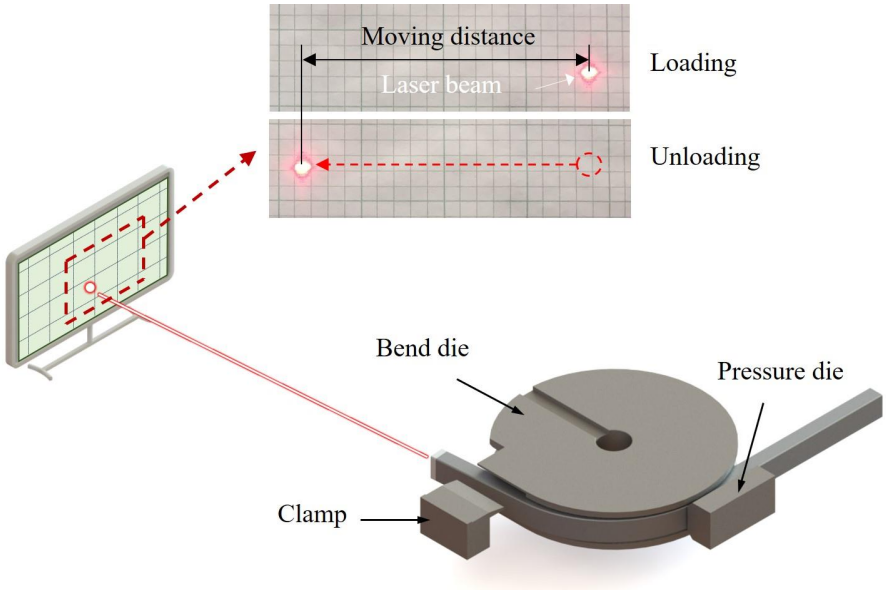

Figure 2.1. Schematic of in-line springback measurement

Ferreira et al. [40] developed a springback evaluation technique for stamping with image processing. The filtered workpiece image was used to evaluate springback angle. In this research, instead of detecting the workpiece shape, the digital image-based laser tracking was integrated into the laser measurement method to measure springback angle for on-machine measurement in real time, as shown in Figure 2.2. An affordable webcam connected to a computer was used for image acquisition, and the acquired images with 30 frames per second (fps) were analyzed to calculate springback angle in real time; every single image frame has a

single laser-beam spot being projected on the datum board. The beam spot reflects geometric change of the sample as reference in the machine.

A laser fitment is made up of a Class 2 laser and an adaptor to hold the laser, which is installed into the aluminum profile before the bending process. The wavelength of the laser used is red-colored 635 nm and the power is 1 mW. This laser is the same as that in a laser pointer and is safe for industrial operation when laser safety guidelines are followed. The device for image acquisition can be positioned in various ways. However, it was set in front of a datum board to avoid perspective images for less image processing, and directly linked to a computer for image acquisition, processing, and springback calculation in real time.

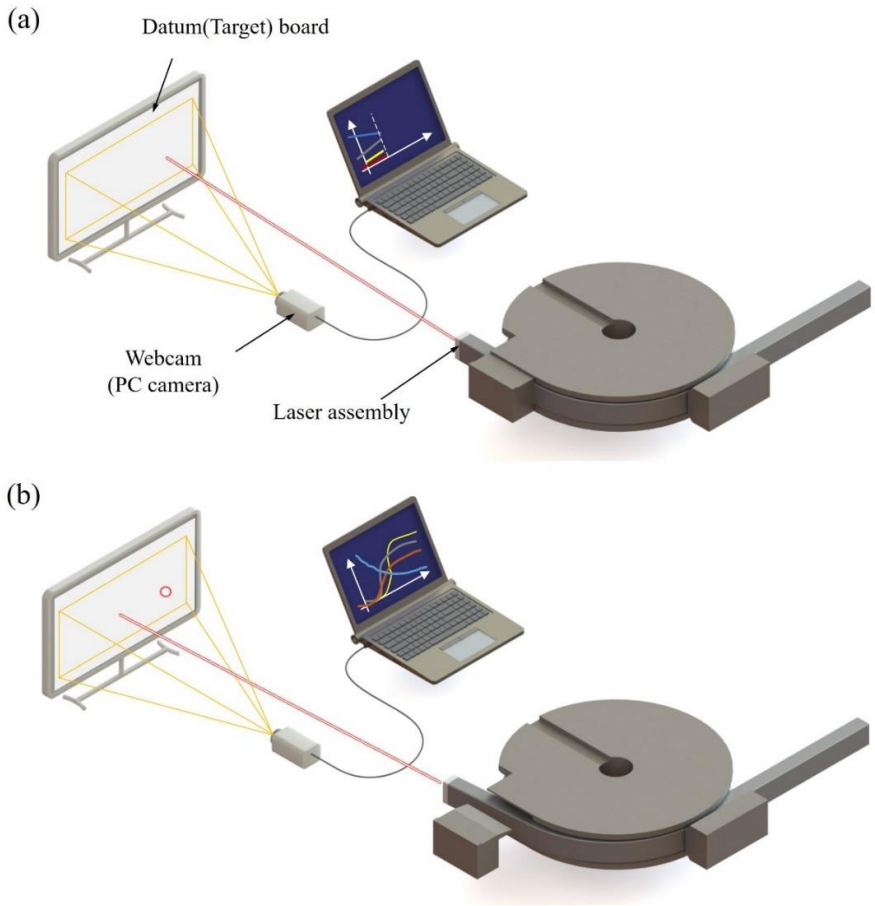

Figure 2.2. Schematic of real-time springback measurement, (a) loading; (b) unloading

Figure 2.3 shows a schematic image with 640×480 resolution, which is displayed on a computer monitor. The laser-beam spot on the image was captured with a rectangular bounding box and a crosshair. The bounding box indicates the location of the laser beam, and the crosshair describes the centroid of the laser beam. The centroid as a beam location was used for tracking a laser beam. Only one laser beam, detected by image processing, is shown in the actual image. The beam moves from right to left on the datum board in Figure 2.3, as the tube springs back after unloading. The location of the captured laser beam upon final loading and after unloading, respectively, is tracked, and the moving distance is used to calculate the springback angle. The 50 mm long reference line on the datum board (see Figure 2.3) is used for converting from the laser beam travelling on the computer monitor to the actual distance on the datum board. In other words, calculating the distance per pixel enables the tracking of laser beam motion on the datum board.

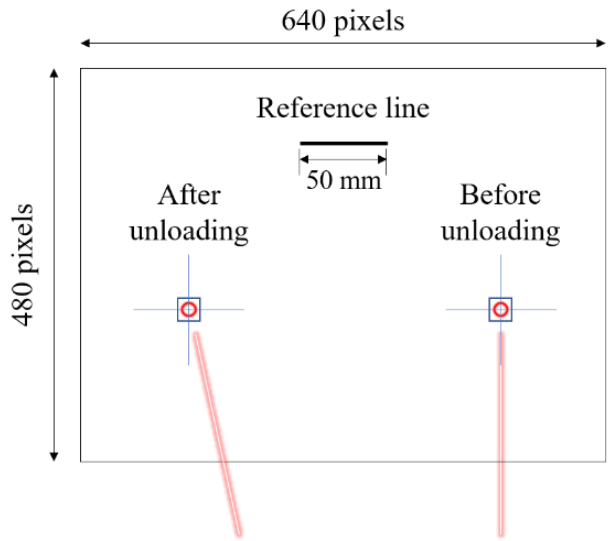

Figure 2.3. Schematic of a laser tracking image

2.3. Springback measurement approach in rotary draw bending process

2.3.1. Digital image processing for laser beam tracking

A color image has three-dimensional color information being allocated to each pixel of the image. For a single channel image processing, the three-color components are quantized to the grayscale which only has a light intensity with an 8-bit depth. Image quantization is a process for dimensional reduction to grayscale, thus it allows each pixel to get a single light intensity and one-dimensional information. Converting color to grayscale is also referred as image decolorization.

The luminance method [41] or weighted method considering the brightness perception of human eye is one of the converting algorithm, which is widely used for converting a color image into a grayscale image. Luminance by Recommendation ITU-R BT.601-7 is the combination of red, green, and blue (RGB) channels with each weighting as follows:

$$I = 0.299R + 0.587G + 0.114B \tag{2.1}$$

Each pixel of a color image is composed of RGB channels, however, the grayscale luminance of the i^{th} frame by Eq. (2.1) can be represented by

$$I_i(x,y) = \begin{bmatrix} I(0,0) & \cdots & I(0,n-1) \\ \vdots & \ddots & \vdots \\ I(a-1,0) & \cdots & I(a-1,b-1) \end{bmatrix} \tag{2.2}$$

where I is pixel intensity, i is the number of image frames, x and y are spatial coordinates, and a and b represent pixels of an image resolution.

As mentioned, a reference line was marked on the datum board to calculate the distance per pixel. The filtered grayscale image of a datum board with a reference line was segmented with the global thresholding technique [42] for background subtraction [43,44]. Figure 2.4 shows the image histogram of Figure 2.5(a) and the threshold is indicated for image filtering. The segmented image, $G(x,y)$, by thresholding is expressed as follows:

$$G(x,y) = \begin{cases} 1 & \text{if I}(x,y) > \text{Threshold} \\ 0 & \text{otherwise.} \end{cases} \tag{2.3}$$

While image thresholding with a fixed level is not suitable to divide the interested region from the image background [45], a fixed-level threshold in Figure 2.5 was used for image segmentation due to the simple background of the datum board. Based on the image histogram

of Figure 2.4, a grayscale image and a segmented image after thresholding are shown in Figure 2.5.

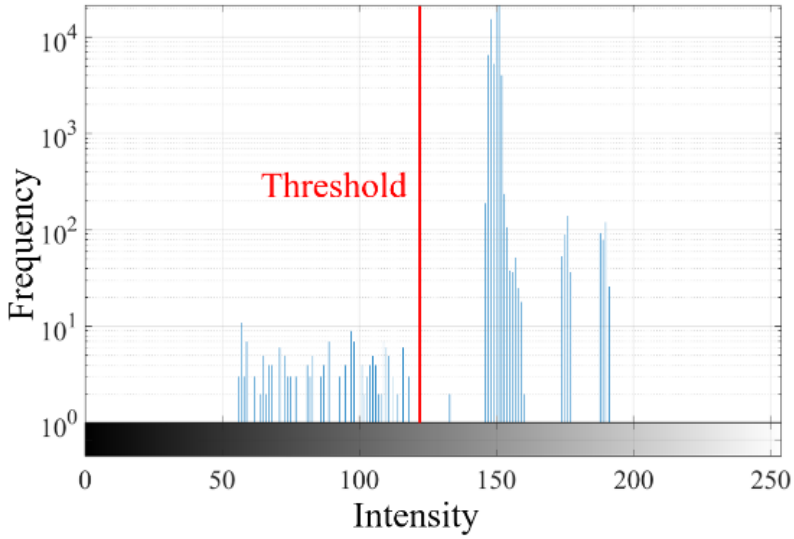

Figure 2.4. Image histogram of the grayscale image

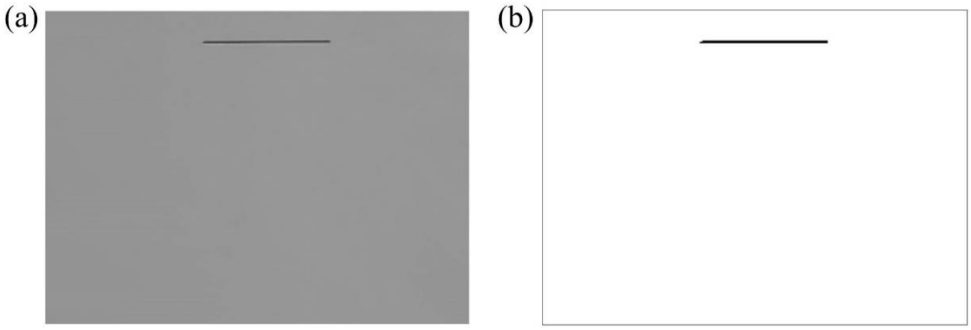

Figure 2.5. Image thresholding, (a) grayscale; (b) segmented image

To remove unnecessary noise for object detection, the region of interest (ROI) for the reference line shown in Figure 2.6(a) was extracted from the image background. The extracted ROI was converted to grayscale using Eq. (2.1). Figure 2.6 presents the ROI of the original image and the reference line surrounded by a bounding box. The number of pixels in the reference line was calculated by the diagonal length of the bounding box. Instead of longitudinal length in the bounding box, the diagonal length was used to reduce errors from a skewed image. The actual

laser moving distance on the datum board can be computed based on the distance per pixel of the prescribed reference line on the computer monitor.

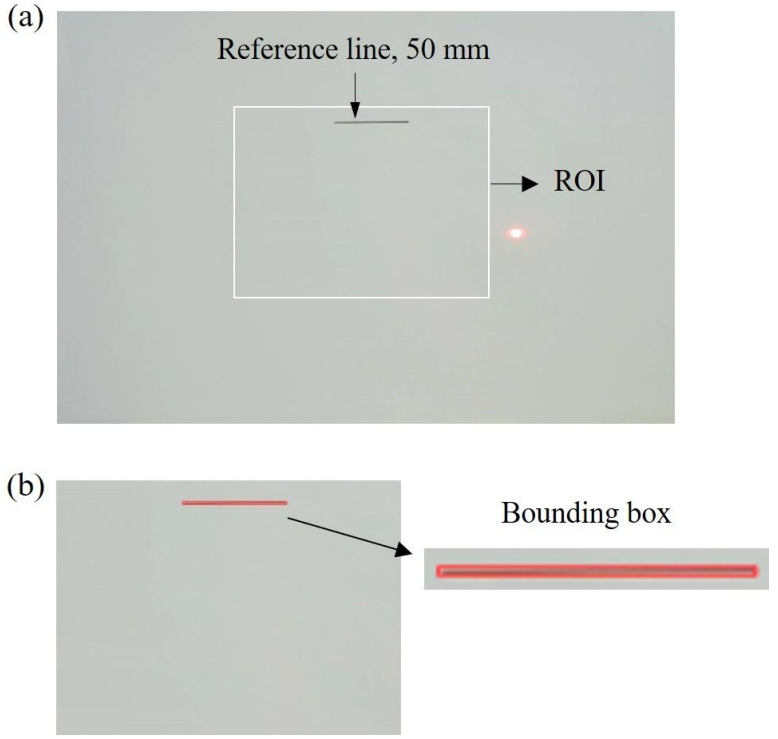

Figure 2.6. (a) ROI of the original image; (b) bounding box of the ref. line

In the same manner as the above technique, the image frame for the laser beam was also converted to the grayscale and binary image. The segmented binary image has a background with 0 and a laser beam with 1. The target object is recognized by the binary information, and the object is being tracked. The goal of object tracking is to obtain its trajectory of every input frame by image processing [46]. A target object of an image frame can be represented by a centroid for object tracking. The centroid of the laser beam intensity was computed based on the binarized image. The centroid of a spatial coordinate, $C(\bar{x}, \bar{y})$, is given by

$$\bar{x} = \frac{\sum_x \sum_y x \cdot I(x,y)}{\sum_x \sum_y I(x,y)}, \quad \bar{y} = \frac{\sum_x \sum_y y \cdot I(x,y)}{\sum_x \sum_y I(x,y)} \tag{2.4}$$

The laser beam movement on the datum board upon springback is found by the difference in the centroid position after springback compared to the initial position of the centroid. The laser moving distance per frame can be evaluated by the Euclidean distance of the centroid between the i^{th} and $(i+1)^{th}$ frames. Therefore, the laser moving distance, d, in real time is computed by

$$d = \sum \left\| C(\bar{x}, \bar{y})_{i+1} - C(\bar{x}, \bar{y})_i \right\| \tag{2.5}$$

The image processing for laser detection and tacking is shown in Figure 2.7. Here, Figure 2.7(a) is the input frame, Figure 2.7(b) is the image converted to 8-bit grayscale, Figure 2.7(c) it the binary image to identify an object, and Figure 2.7(d) is the output frame through image segmentation and filtering. The fully converted image, Figure 2.7(d), is used to display the laser beam position and to acquire the desired data. As mentioned above, the centroid which is an intersection of the crosshair in Figure 2.7(d) is tracked, and the centroid position is logged in real time.

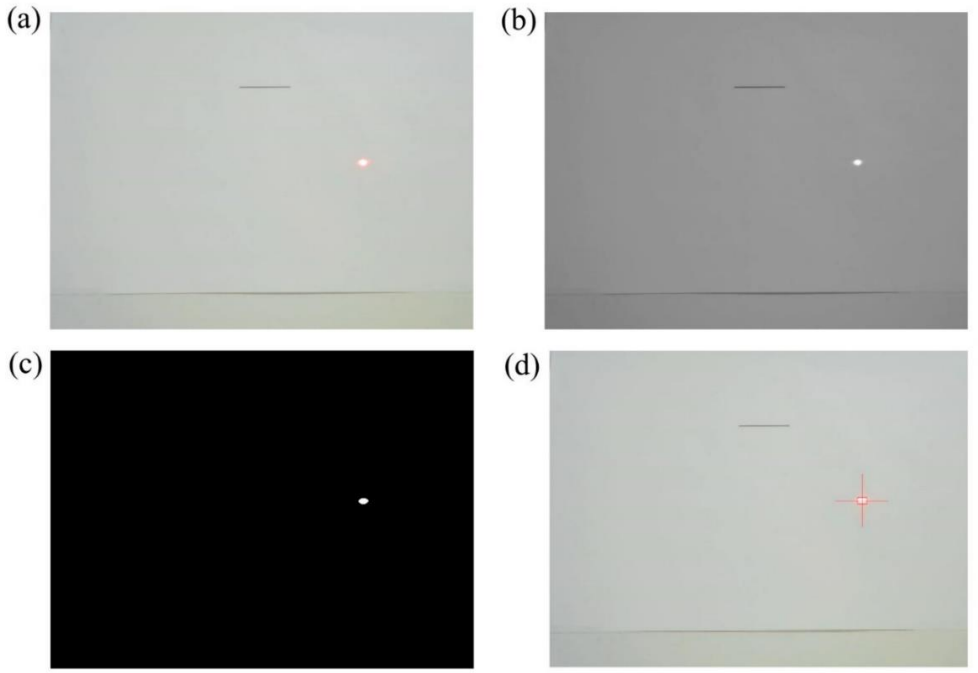

Figure 2.7. (a) Original image; (b) grayscale; (c) binary; (d) laser beam detection

In the algorithm for real-time springback measurement, there are two different image processing groups to calculate the laser beam position, as shown in Figure 2.8. The first group

is for the reference line, and the second group is for the laser beam tracking. Since the position of the image acquisition device, a webcam of Figure 2.2, was not fixed, computing the distance per pixel of the reference line prior to laser beam tracking was required during setup. While image processing for the reference line is run once, image processing for laser beam tracking iterates until the end of image acquisition. The laser beam tracking can be performed by synthesizing two image processing algorithms.

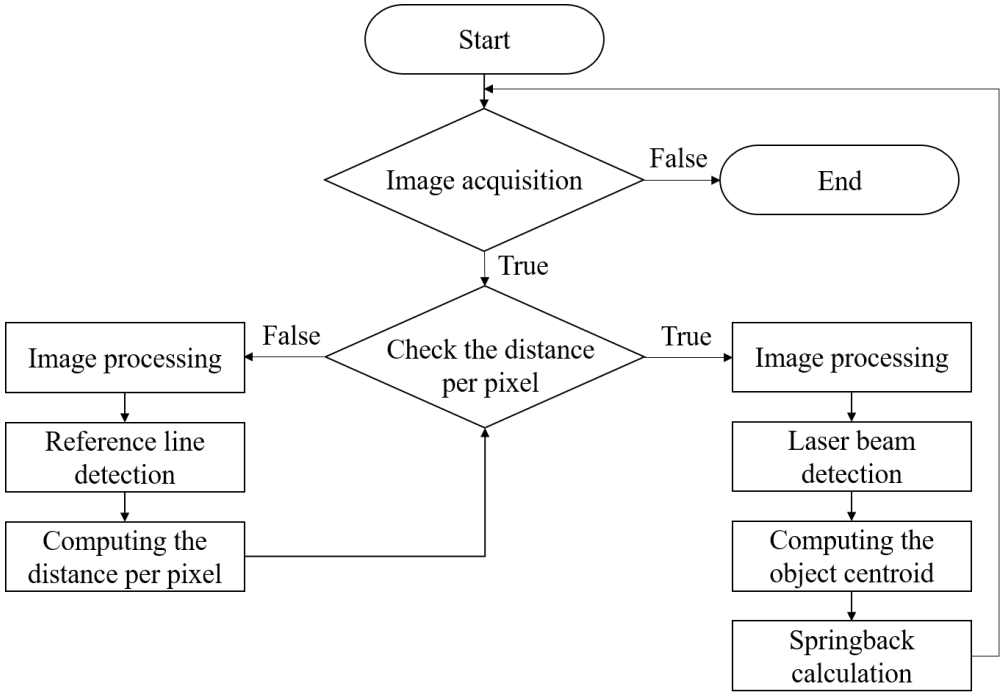

Figure 2.8. Image processing flow for laser beam tracking

2.3.2. Geometric calculation of springback

The springback angle, $\Delta\theta$, in Figure 2.9 is taken as the difference between bending angle before unloading θ_{initial} and released bending angle θ_{final}. $\overline{A'B}$ is the datum board distance from the neutral axis of the unbent tube, $\overline{AC}$ is the imaginary line of the profile's neutral axis after unloading, and $\overline{BC}$ is the actual moving distance of the laser beam on the datum board. The springback angle $\angle CAB$ can be calculated by trigonometry, which is given by

$$\Delta\theta = \arctan(\frac{\overline{BC}}{\overline{AB}}) \text{ or } \Delta\theta = \arctan(\frac{\overline{BC'}}{\overline{A'B}}) \tag{2.6}$$

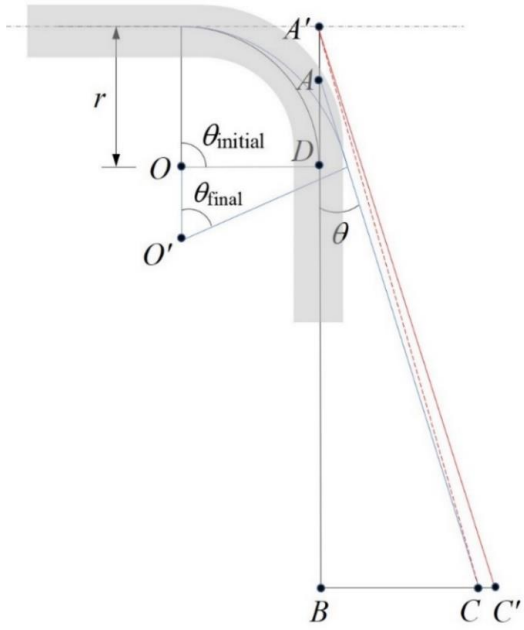

Figure 2.9. Springback geometry of profile bending

Geometrically, the location of point A is unknown due to the unknown released bend angle, θ_{final}. To overcome uncertainty and reduce the calculation error, Ha et al. [38] computed the springback angle by creating an imaginary line $\overline{A'C'}$ parallel to $\overline{AC}$ and updating a calibration distance $\overline{CC'}$ based on an initial bent angle $\angle CA'B$. $\overline{A'C}$ moves towards $\overline{A'C'}$ by updating the calibration distance as follows

$$\overline{CC'} = \frac{\sin(\theta_{\text{initial}}(1-\eta))}{\cos(\theta_{\text{initial1}}\eta)}\left[\frac{r(\sec\theta_{\text{initial}}-1)}{\tan\theta_{\text{initial}}} - \frac{r\{\sec(\theta_{\text{initial}}(1-\eta))-1\}}{(1-\eta)\tan(\theta_{\text{initial}}(1-\eta))}\right] \tag{2.7}$$

where r is bending radius, θ_1 is bend angle, and η is springback ratio given by

$$\eta = \frac{\Delta\theta}{\theta_{\text{initial}}} \tag{2.8}$$

The calibration distance is assumed sufficiently small, compared to the laser moving distance, $\overline{BC}$, to be neglected in the springback calculation. Then, the springback angle is approximated by

$$\Delta\theta = \arctan\left(\frac{\sum\left\|C(\bar{x},\bar{y})_{i+1} - C(\bar{x},\bar{y})_i\right\|}{\overline{A'B}}\right) \tag{2.9}$$

2.4. Experiment and Discussions

2.4.1. Experimental set-up

The material used for RDB was the AA6082-T4 hollow rectangular tube with exterior dimensions 60 × 40 mm and thickness of 3 mm. The bend die radius was 252 mm, and the bending angles were 30º, 45º, 60º, and 90º. Three workpieces (950 mm long) were used for each bending angle. The datum board was installed at 3.0 m distance from the point O in Figure 2.9, the center of the bending radius.

A laptop computer with i5-7200U 2.5GHz and 8GB memory was employed to realize a tracking system. A webcam with 720p (1280×720) and 30 fps connected to the computer acquired images during the unloading process. The image processing was performed in MATLAB. For each bending process, 90 frames with 640×480 true color (24 bits) images were obtained at a rate of about 10 fps, and were used to track the laser beam of the datum board in real time.

Figure 2.10(a) illustrates the overall experimental system viewed from the tube. The enlarged image displays the reference line and the laser beam on the datum board. A laser fitment was installed at the tip of the hollow profile shown in Figure 2.10(b). The laser beam was used for the indicator of the profile's longitudinal direction on the datum board. As noted above, the laser beam on the datum board was tracked by the image processing algorithm. The springback angle, θ, in Figure 2.10(b) was manually measured without taking the workpiece from the machine to compare the springback to on-machine measurement. Since RDB was conducted without mandrel and wiper die in the experiments, it was assumed that springback only occurs in the bent part, which eliminates any effect of the absence of wiper die and mandrel after unloading.

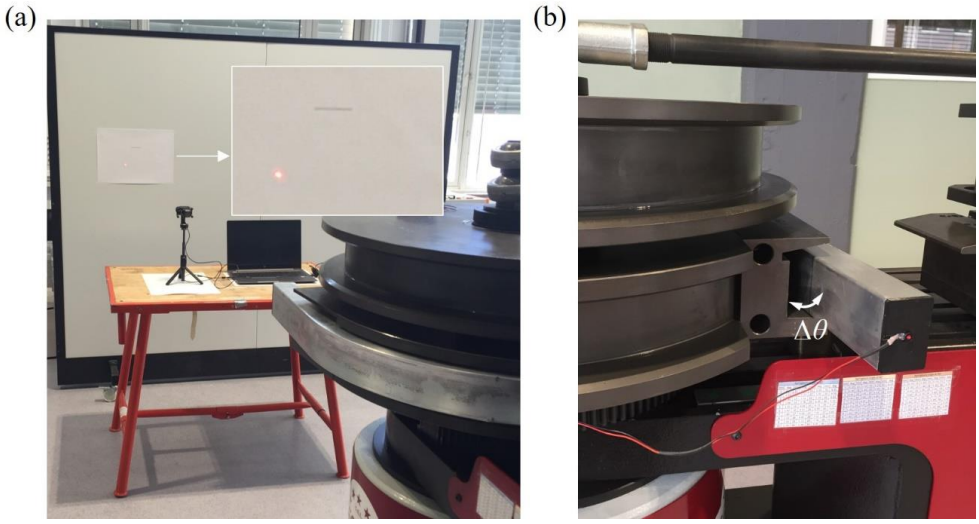

Figure 2.10. Experimental set-up, (a) view from a tube; (b) bent tube

Springback can be calculated with a robust prediction model. However, springback is affected by complex process conditions such as material properties, geometry, lubrication, bending speed, and tooling, geometry. Since precise springback prediction is not an easy task, springback measurement is of great importance to control product quality and compensate springback.

Two different measurement methods were adopted for the springback measurement. Firstly, manual measurement of springback was carried out without removing the workpiece from the bending machine to verify the on-machine springback measurement in real time. The tube shapes at 30º, 45º, 60º, and 90º bending angles are shown in Figure 2.11.

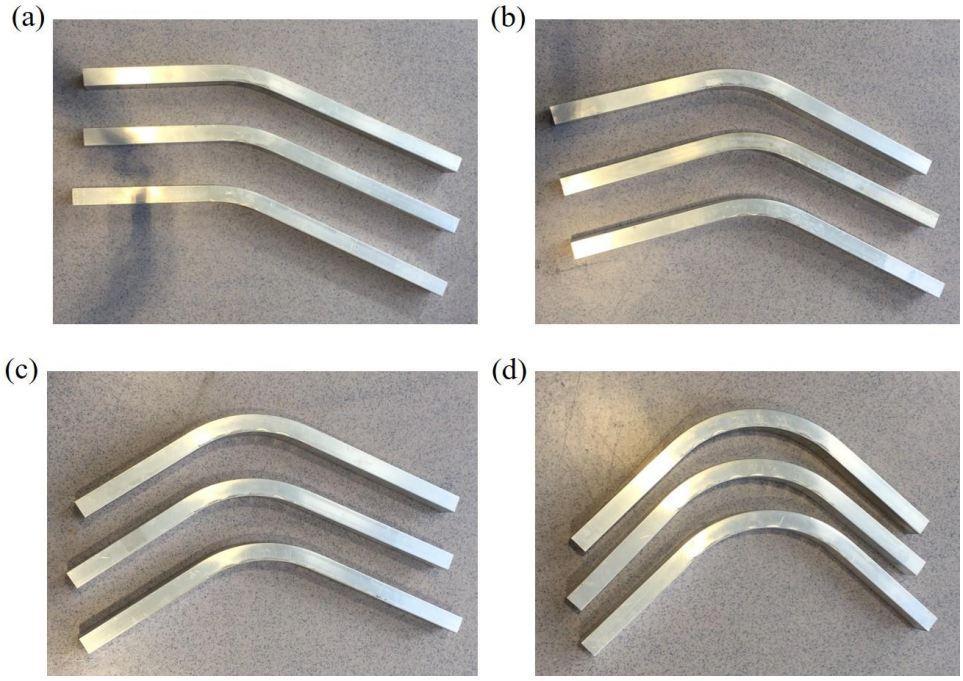

Figure 2.11. Experimental workpieces, (a) 30º; (b) 45º; (c) 60º; (d) 90º bending

Secondly, the springback angle was monitored and measured in real time during the unloading process. This on-machine measurement method serves the purpose of measuring the springback angle by digital image-based laser tracking, without transferring the workpiece for springback measurement. The image processing algorithm was run after each bending process, before the clamp was released and unloading performed.

The on-machine measurement results of springback are plotted in Figure 2.12. Each graph has real-time springback data of three workpieces. The x-axis indicates the frame number, and the y-axis indicates the springback angle. The webcam had a 30 Hz frame rate. Due to the time spent on image processing, the output frame rate after image process became 10 Hz. The gray-colored circle in Figure 2.12 is the starting point of unloading, as the clamp after bending was randomly released. Each profile was fully recovered in two or three frames after unloading, and the springback angle was rapidly increased and converged after unloading. The slope of springback also increased, as the bending angle increased. However, the sharp edges after unloading were shown in the 30º bend angle in Figure 2.12(a) because the clamp bumped against a stopper when it was fully released. The peak point was stabilized and converged fast. Accordingly, the effect of the clamp releasing vibration is considered negligible. The on-

machine measurement graphs display that the image tracking algorithm follows the laser beam in real time, and tubes are less bent than the desired bending angle due to elastic recovery.

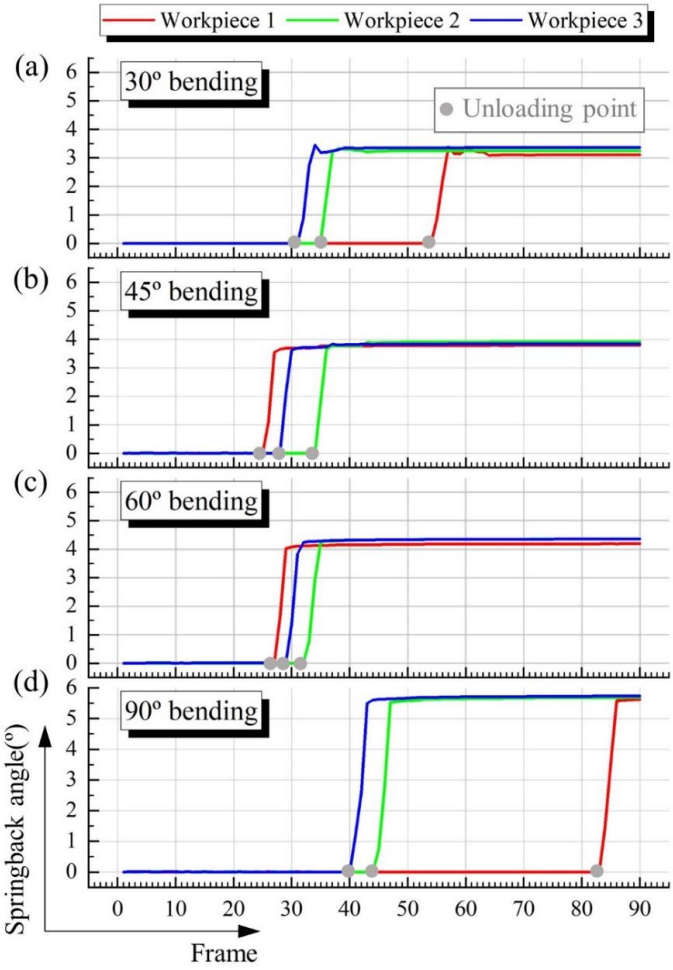

Figure 2.12. On-machine springback measurement in real time

As an example of the image processing for on-machine springback measurement, the original and tracking images for 90º bending are shown in Figure 2.13. The images in Figure 2.13(a) are the raw images from the image acquisition device, and Figure 2.13(b) shows the object captured images by object tracking in real time. The laser beam was located on the right side of the datum board as the initial position before unloading in the 1st frame. Unloading started at the 44th frame, and the laser beam moved from the 45th to the 48th frames. The final position of

the laser beam is shown in the 90th frame. While the springback angle was calculated with the final laser position of the 90th frame based on the 90 input images, the real-time monitoring can also apply to determine the status of loading and unloading for on-machine springback measurement.

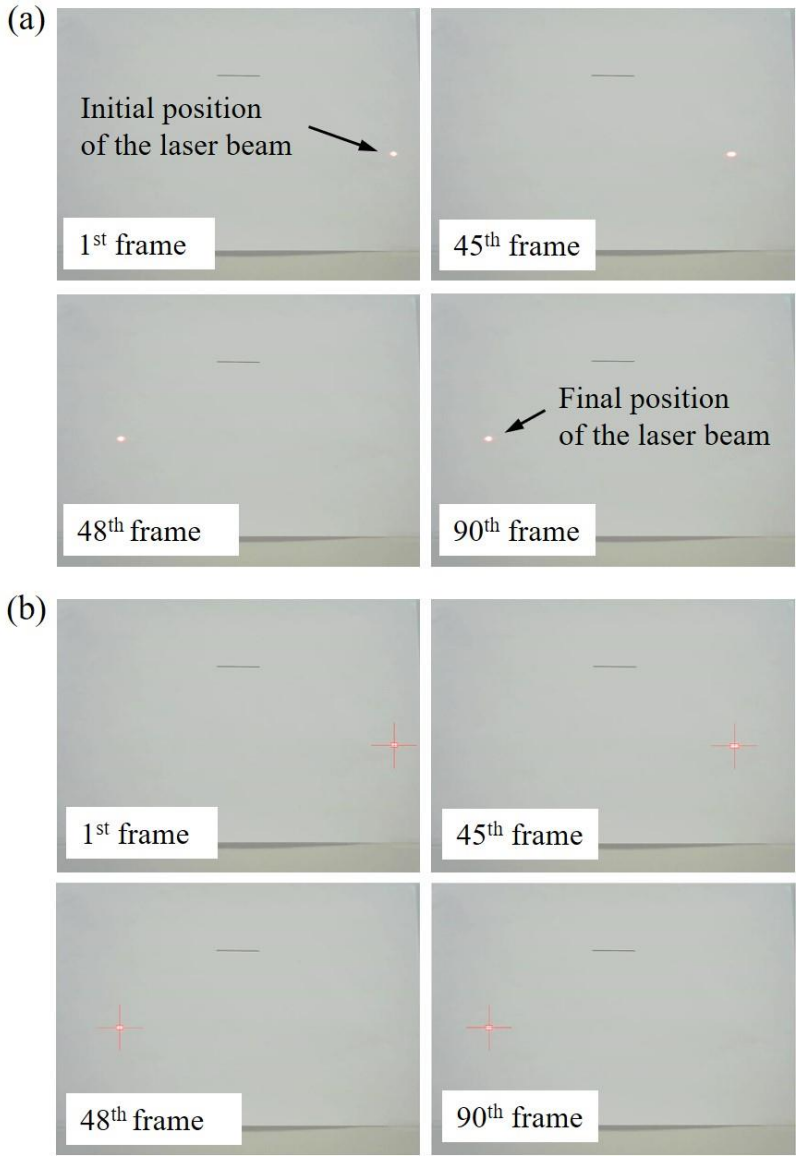

Figure 2.13. Laser beam tracking, (a) original image; (b) tracking image

2.4.2. Measurement results

According to the image processing flow presented in Section 2.3, the springback was logged on the computer during the unloading process, and the springback was also manually measured after springback. The springback angles by on-machine measurements are listed with the manual measurement results in Table 2.1. Both measurements show that the springback increases with an increasing bend angle from 30º to 90º. However, the standard deviation (SD) of the manual measurement is mostly higher than the image processing results. The average SD of the manual and on-machine measurements are 0.12º and 0.09º, respectively.

Table 2.1. Springback measurement results (unit: degree)

Measurement	Workpiece	Bending angle			
		30º	45º	60º	90º
Manual	1	2.99	3.68	4.31	5.51
	2	3.05	3.80	4.27	5.77
	3	3.31	3.77	4.44	5.57
	Average ①	3.12	3.75	4.34	5.62
	Stand. Dev.	0.17	0.06	0.09	0.14
On-machine	1	3.11	3.80	4.19	5.62
	2	3.25	3.93	4.37	5.69
	3	3.37	3.85	4.36	5.74
	Average ②	3.24	3.86	4.31	5.68
	Stand. Dev.	0.13	0.07	0.10	0.06
Difference |①-②|		0.12	0.11	0.03	0.06

The springback results are plotted with bar charts in Figure 2.14. A line with two filled circles at its end is the relative difference slope between two different measurements based on the same workpiece. The maximum observed difference is 0.20º of workpiece 2 in 30º bending, and the minimum is 0.06º of workpiece 3 in 30º bending. For workpiece 1 bent at 90º, while the clamp was released at the 83rd frame as shown in Figure 2.12 and the data logging was finished at 90th frame, the springback from the on-machine measurement was 0.11º slightly higher than the manual measurement. It is considered that the unloading point does not critically affect the springback measurement. The springback difference of each workpiece had no particular trend, but the overall differences between manual and on-machine measurements were within +0.20º/-0.12º.

The averages of the springback angles and the differences between the two measurement techniques are plotted in Figure 2.15. From the error bars in Figure 2.15(a), it can be observed that the variation of the measured springback angles, manual or on-machine, are very small. The springback values, as expected, increased as the bending angles increased due to elastic recovery of the material. Since the differences between the averaged manual and on-machine measurements were within 0.12º for different bending angles ranging from 30° to 90°, the on-machine measurement based on image processing captured the springback trend well. The on-machine springback measurement data in Figure 2.14 and Figure 2.15 show that there is no appreciable difference comparing the two methods through four different bend angles with three samples for each angle. With these validation results, the on-machine measurement by image processing appears to be a feasible springback measurement strategy for profile bending.

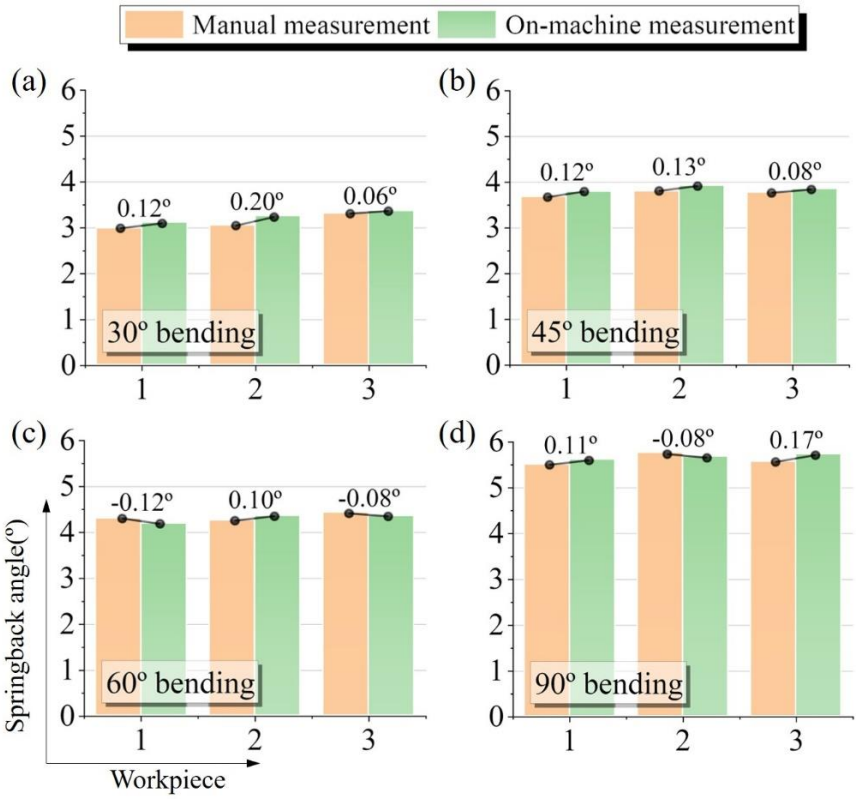

Figure 2.14. Springback comparison based on each workpiece

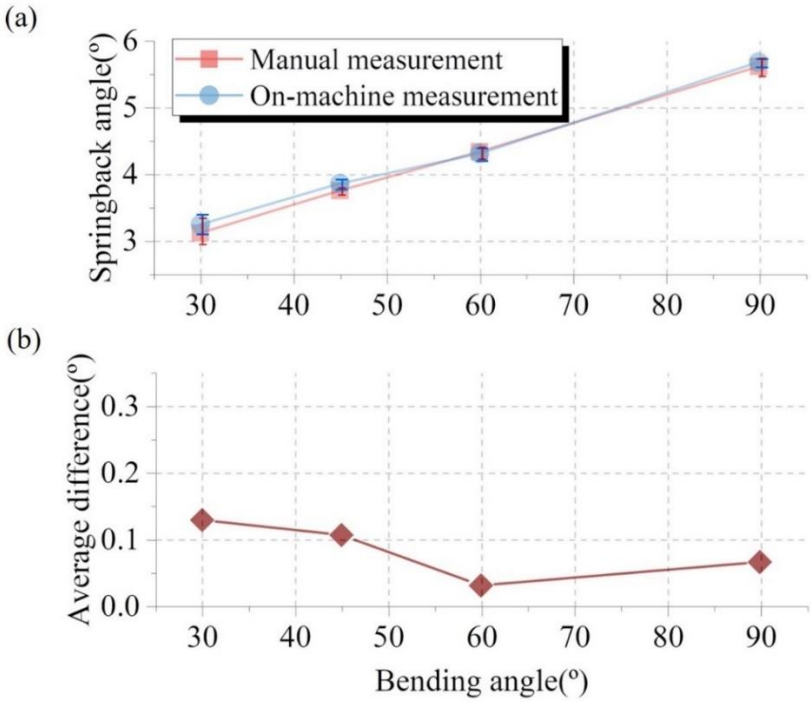

Figure 2.15. (a) Average springback angle; (b) difference between the averaged manual and on-machine measurements

2.5. Conclusions

In this paper, a cost-effective system for on-machine springback measurement in RDB has been developed using digital image processing and laser tracking. The system was integrated with a 635 nm laser, an affordable image acquisition device, and an image processing technology. Springback was evaluated in real time, while eliminating the need for transferring the workpiece to an off-line measurement device.

The newly developed measurement method was applied to AA6082-T4 rectangular tube bending at 30º, 45º, 60º, and 90º. A target board to display a laser beam was set at 3.0 m from the center of a bend die. Every color image acquired by a webcam was quantized to a grayscale with the intensity value ranging from 0 to 255. Then, the grayscale was binarized by thresholding based on the image histogram to extract the laser beam from the image background. The springback angle was calculated by updating the beam location of the images. The performance of the on-machine measurement method was validated by comparing to conventional manual measurements. The average SD of the on-machine measurement was 0.09º ranging from 0.06º to 0.13º while the corresponding value for manual measurement was about 0.12º. The differences between the averaged manual and on-machine measurements were within 0.12º ranging from 0.03º to 0.12º, and the on-machine measurement was found to be in a good agreement with the manual measurement. The affordable hardware system and tracking algorithm based on MATLAB were sufficient to capture the physical springback angle compared to the manually measured data.

The measurement strategy with integration of a laser and an image processing technology enables a bending process to be monitored in real time and the springback angles to be measured on a tube bending machine. Thus, the present approach provides an attractive measurement technique that can be adopted to improve manufacturing efficiency. For implementation, the laser and camera hardware are easily available. With hardware connection, the laser beam detection, object tracking, and springback calculation programs can be executed in a computer to collect springback data for progress control in a smart manufacturing environment. The digital images and the extracted springback data can be stored in a cloud data platform and become an essential component of a data-driven decision system where product quality is predicated. The on-machine measurement and real-time process monitoring technology can facilitate manufacturing digital transformation towards Industry 4.0.

3. A computer vision-based, in-situ springback monitoring technique for bending of large profiles[**]

3.1. Introduction

The progress in the metal forming technology has been driven by with growth of automotive, aerospace, shipbuilding, and manufacturing infrastructure. Different complex products using metal forming are widely used in the subframe, product skin, product component, and so on. Once a formed product is used as a component of an assembly, its dimensional accuracy based on assembly tolerances affects product assembly of components and quality control [47]. Springback is an inevitable phenomenon under certain metal forming conditions. It is an important factor which decreases geometrical accuracy and reduces product quality if not controlled properly. While many theoretical approaches have been developed to predict springback, these are not fully capable of representing the actual forming process due to the process complexity and parameter uncertainty [48]. Several factors of forming processes—i.e., material and machine condition, manufacturing environment, etc.—can cause geometrical variability due to springback.

Geometric measurement after metal forming is usually the first step in understanding the geometric accuracy by springback. Many researchers have studied springback measurement methods, such as non-contact measurement. A laser beam as a non-contact method was proposed to measure springback in rotary draw bending by Ha et al. [38]. They used a laser assembly fitted at the tip of a circular profile, making a reference for the longitudinal direction of a profile during bending. The location change of a laser beam by a springback phenomenon was shown on the target board. By reading the change of laser beam locations between loading and unloading, the springback angle was obtained with the trigonometric calculation. Ghiotti et al. [35] proposed a springback measurement technique in roll bending using an inertia measurement unit (IMU) attached to a mandrel. The angular velocity and acceleration data were acquired by the IMU, and the bend radii and springback factor were calculated. Hamedon et al. [49] introduced a deformation measurement technique by adopting a borescope attached to a

[**] * Reprinted with permission from T. Ha, J. Ma, J. Blindheim, T. Welo, G. Ringen, J. Wang, A computer vision-based, in-situ springback monitoring technique for bending of large profiles, ESAFORM 2021, Liège, Belgique: ULiège Library; 2021

stamping die. A 90° folding mirror was added to overcome a space constraint and acquire image frames of a workpiece. The geometrical status, i.e. deformation, wrinkling, and springback of a workpiece in stamping, can be monitored in real time. However, an additional piece of equipment for protecting a sensor from e.g., high temperature or lubrication of a die is necessary under certain circumstances. Ferreira et al. [50] integrated an image processing into a press controller to calculate springback angle during forming operations. The original image was converted and filtered to obtain a binary image of an aluminum alloy sheet. The binary image was divided into two frames of left and right edges, and then the springback angle was calculated by detecting two extreme points of the edge to make a reference line of the sheet metal.

The aforementioned measurement methods do not need physical contact to measure geometry in real time. Nevertheless, those methods require a location to install a sensor to a forming system, or an extra component to protect a sensor [35,38,49]; simple image background can be necessary to easily detect the edge of sheet metal [50].

To overcome limitations associated with image processing in metal forming, this present work presents a springback measurement technique by computer vision used under complex and heavy-noise image background. Three points on the side of a profile were marked on prescribed locations, and a simple cell phone camera was used for image acquisition. The image processing was based on the stretch bending process of a large profile in real time. Local point tracking was applied to follow the deformation of the profile instead of a global search of the image.

The remainder of this paper is organized as follows: An overview of the stretch bending machine for experiments is presented in the Section 3.2. Springback measurement for a large profile is introduced in Section 3.3. The measurement validation of the computer vision and conclusions are addressed in Sections 3.4 and 3.5, respectively.

3.2. Three-dimensional (3D) stretch bending

A rectangular hollow profile of length 1,900 mm is used in the three-dimensional stretch bending machine, shown in Figure 3.1. Unlike transverse die forces applied to the profile [51,52], rotating dies are used for stretch bending in this machine. The bending machine has two sets of a two-axes gimbal system, and the rotating pivots of each gimbal are orthogonal. It has five degrees of freedom (DOFs) for stretching and bending. 1 DOF serves to stretch the profile in the horizontal direction, other 2 DOFs enable bending in the horizontal direction, and the other 2 DOFs enable bending in the vertical direction. Each arm is symmetrically set. The arms can be independently controlled in 5 DOFs, providing product flexibility. The bending die is three-dimensional; thus, the profile can be bent in vertical and horizontal directions. Moreover, several sensors, i.e. position and torque, are used to monitor the process and provide feedback to the control system.

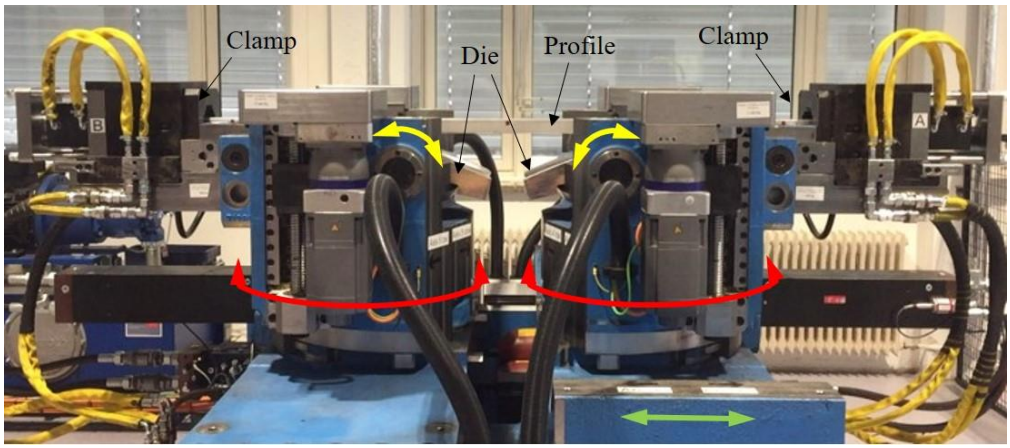

Figure 3.1. 3D stretch bending machine

The machine operations in translation (green arrow) and horizontal bending (red arrows) are controlled by hydraulic forces. The yellow lines of the machine in Figure 3.1 are the hydraulic hoses. On the other hand, machine operations in vertical bending (yellow arrows) are controlled by servomotors and ball screws. A profile installed into the die is clamped at the ends. Thus, the hydraulic clamping system with an insert constrains the profile. The right arm base is translated to prestretch the profile until the prescribed time and position are reached. Next, the profile is bent in the vertical direction. For 3D bending, as shown in Figure 3.2, the profile is subsequently bent in the horizontal direction. The rotating speeds of all pivots for bending are

also controllable. The clamped profile is released after bending, and then the profile is free to spring back.

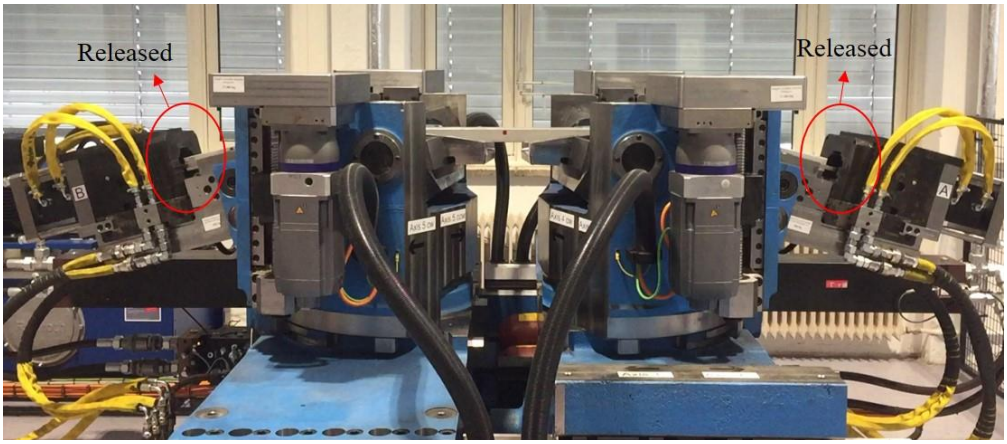

Figure 3.2. 3d profile bending

3.3. Springback measurement procedures

3.3.1. Experimental set-up

AA6082 T-4 hollow profiles were symmetrically bent in the vertical directions (yellow arrows in Figure 3.1). The specific material dimensions and properties are shown in Table 3.1. Since the profile length was 1,900 mm, it is challenging to measure geometry with a coordinate measurement machine (CMM) or a vernier caliper due to the measuring range. While a laser tracker or a 3D scanner is an option to measure such a large-sized object, cost efficiency, measuring accuracy, or measuring resolution can be a problem. To achieve an affordable and feasible measurement, a cell phone camera (iPhone 6) and a laptop computer (i5-7200 CPU 2.5GHz / 8GB RAM) were used for image data acquisition and processing. The acquired color images were 1920 pixels wide and 1080 pixels high. The iPhone 6 camera with a 73° field of view was set up perpendicularly to the machine to avoid skewed images. Figure 3.3 shows the side view of a profile, which has three points. Since point marking is robust to vibration or any other external noise, two points were marked at a prescribed location of 150 mm from each extreme edge and 30 mm from the bottom, while the third point was marked at the center of a profile.

Table 3.1. Material dimensions and properties

Length	1900 mm
Width	60 mm
Height	40 mm
Thickness	3 mm
Elastic modulus	72 GPa
Yield strength	146 MPa
Flow stress (MPa)	$\sigma = 502(0.0092 + \varepsilon_p)^{0.26}$

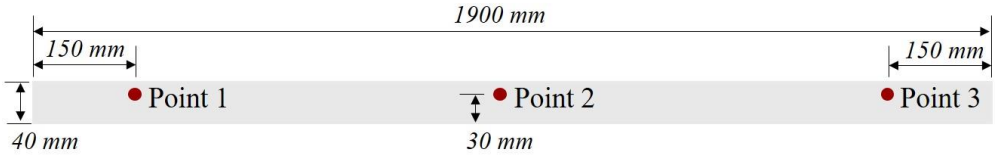

Figure 3.3. Three reference points on the side of a profile

Springback is an elastic recovery phenomenon occurring right after unloading. During the bending process, three image frames are acquired to calculate springback at t_0, t_1, and t_2 in Figure 3.4. t_0 shows the moment that a profile is fully clamped and ready to bend; t_1 shows the moment that a profile is bent to the target angle and ready to be released; t_2 shows the moment that a profile is fully bent and released. Each image frame is segmented and filtered to extract the three reference points. The first image enables transforming the real distance to the distance between the pixels of points 1 and 3 on the image frame. It allows the distance per pixel to be calculated. From the second and third image frames at t_1 and t_2, the deformation status of the bent profile is identified. Springback as shown in Fig. 4 is obtained with the three points marked on the profile.

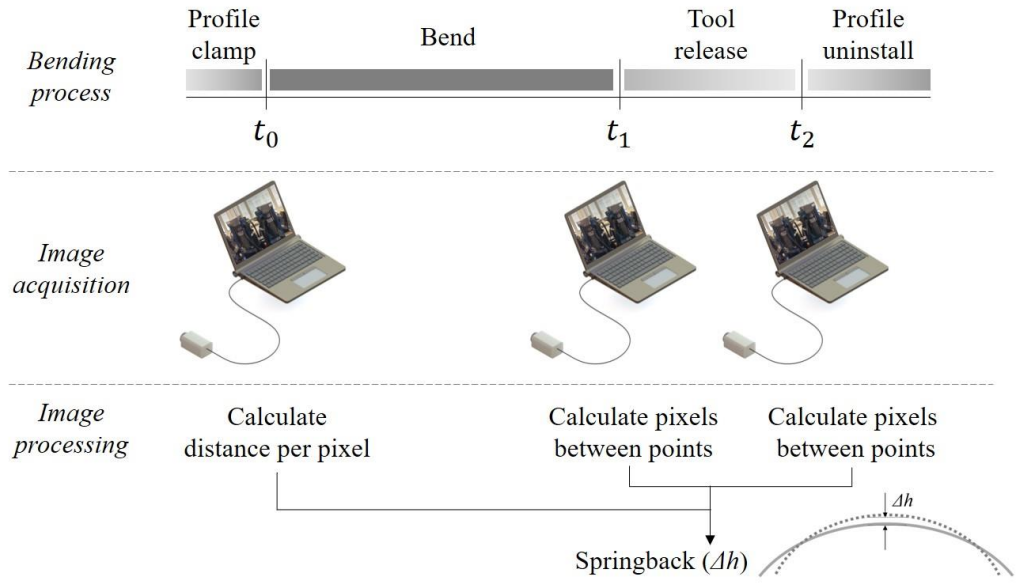

Figure 3.4. In-situ springback monitoring procedures

3.3.2. Image processing for springback measurement

Computer vision technology as a means of sensing has been widely applied to detect, discriminate, recognize, and track an object with high accuracy from food quality evaluation [53] to traffic analysis [54], autonomous driving [55], or exploring space [56]. For the geometrical measurement with computer vision, displacement history of long-span bridges was measured with LED targets and a high-resolution camera [57]; seismic responses of a bridge under the different weight and speed of vehicles were monitored with a vision-based system [58]; digital image correlation (DIC) was also used for deformation measurement of an object surface [59]. Based on such computer vision techniques, springback in metal forming was measured without contacting the workpiece or necessitating removing it from the machine.

The three image frames from the camera were processed within MATLAB environment. Generally, image pre-processing is required to separate a target object from the image background. An image of the manufacturing environment does not possibly provide a clear-background image, and the obtained images may also have a complex and noised background, as shown in the image histogram of Figure 3.5. The intensity of image pixels is broadly distributed, and all image pixels, except for the target object, act as noise for image processing. An advanced algorithm is necessary to detect and extract the points for global object search, an it can require a high-performance hardware and a lot of computation time.

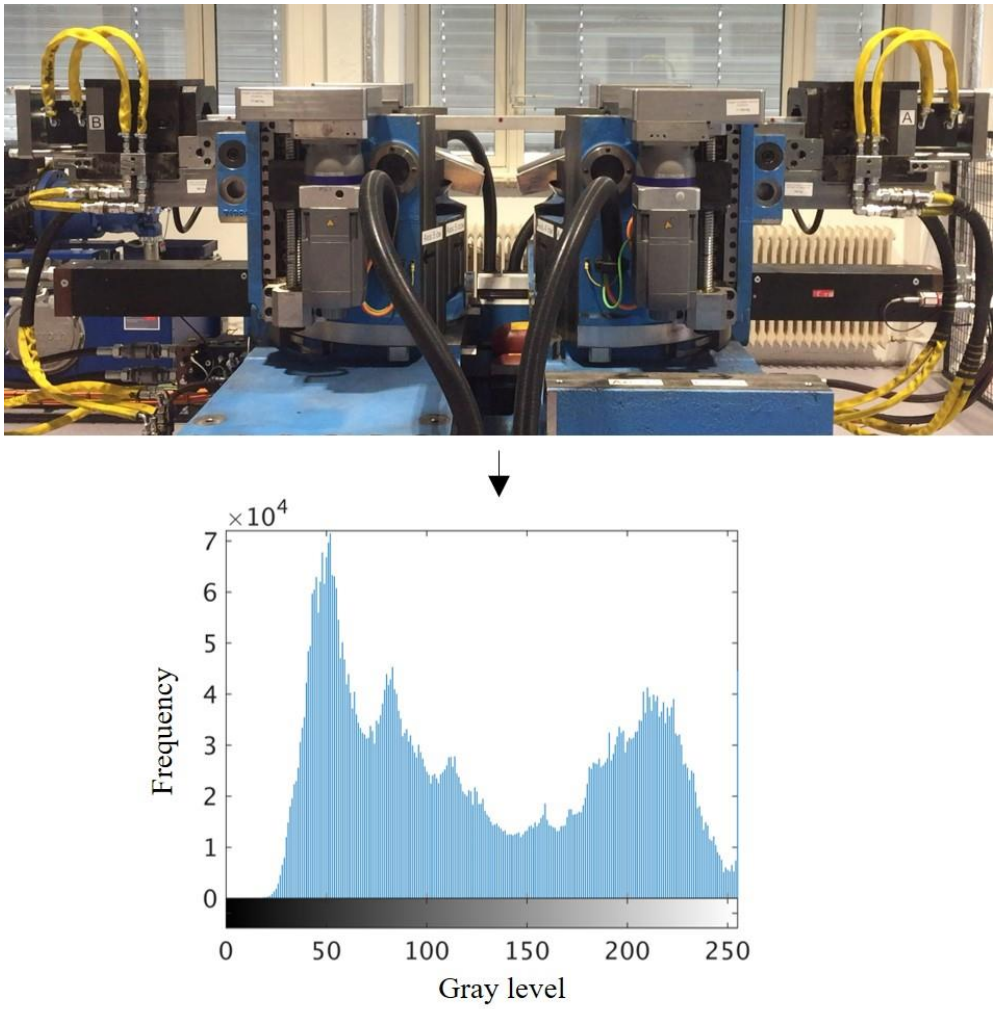

Figure 3.5. Gray-level histogram of the image

To avoid background noise, a local search instead of a global one was used by segmenting a region of interest (ROI). The converted gray-scaled image is expressed as

$$I_G(x,y)=\begin{bmatrix} I_G(0,0) & \cdots & I_G(0,M-1) \\ \vdots & \begin{bmatrix} I_G(u,v) & \cdots & I_G(u,v+m-1) \\ \vdots & \ddots & \vdots \\ I_G(u+n-1,v) & \cdots & I_G(u+n-1,v+n-1) \end{bmatrix} & \vdots \\ I_G(N-1,0) & \cdots & I_G(N-1,M-1) \end{bmatrix} \tag{3.1}$$

where $I_G(x,y)$ is the image intensity, M and N are image resolution in an image. A matrix in $I_L(x,y)$ represents the intensity of a segmented image for local search of a target object, and it can be expressed as

$$I_L(x_L,y_L)=\begin{bmatrix} I_L(0,0) & \cdots & I_L(0,m-1) \\ \vdots & \ddots & \vdots \\ I_L(n-1,0) & \cdots & I_L(n-1,m-1) \end{bmatrix} \tag{3.2}$$

where m and n are image resolution of the segmented image. A local search strategy reduces computation time. Each element of the local matrix is also transformed into the global coordinate $G(x,y)$, given by

$$G(x,y)=\begin{bmatrix} 1 & 0 & u-1 \\ 0 & 1 & v-1 \\ 0 & 0 & 1 \end{bmatrix}\begin{bmatrix} x_L \\ y_L \\ 1 \end{bmatrix} \tag{3.3}$$

The circle Hough transform (CHT) [60,61] was used to find the point center of a profile in the segmented image. The general equation of a circle centered at (a,b) with radius r is given by

$$(x-a)^2+(y-b)^2=r^2 \tag{3.4}$$

The locus of the center can be expressed in polar coordinates as

$$\begin{cases} a=x-r\cos\theta \\ b=y-r\sin\theta \end{cases} \tag{3.5}$$

The image space is transformed into the parameter space with Eq. (3.5). Figure 3.6 illustrates the CHT concept to search a circle center; black dots are edge pixels, and a triangle is the peak in the parameter space. The parameters, the locus of center and radius, generate many circles in the parameter space along the edge of the image space. The parameter space contains a peak, an overlapped point, which can be represented as the center of the circle.

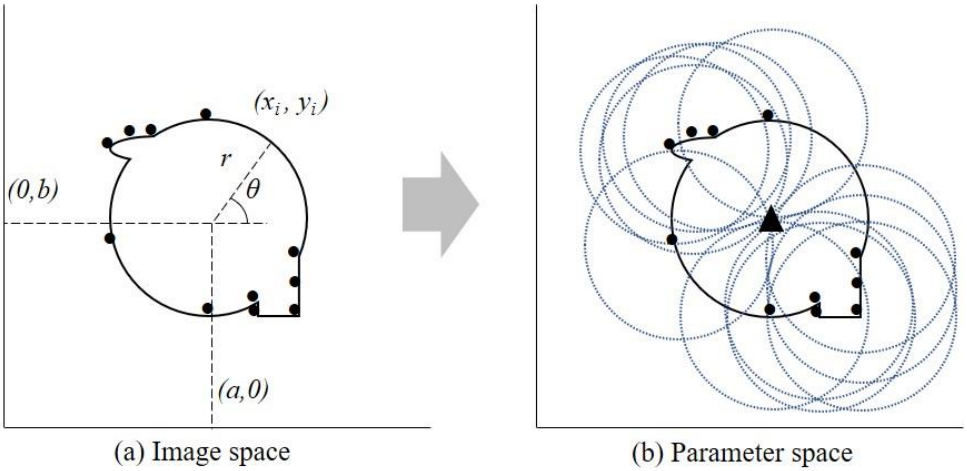

Figure 3.6. Concept of the circular hough transform

Figure 3.7 shows an original image after loading and unloading. As mentioned in Section 3.3.1, the locations of points are predetermined. Three local regions containing a reference point at time t_0, t_1, and t_2 are segmented based on the input bending angle. Red cross-hairs represent locations of reference points by circle detection. In Figure 3.8, the procedure to search a circle on the image is introduced. The first image of points 1, 2, and 3 is the segmentation from the original image; the second image is a gray-scale image; the third image is a binary image by thresholding; the last image shows the circle detection. The local coordinate of the circle searched by the CHT in the fourth image of Figure 3.8 is transformed into the global coordinate given by Eq. (3.3).

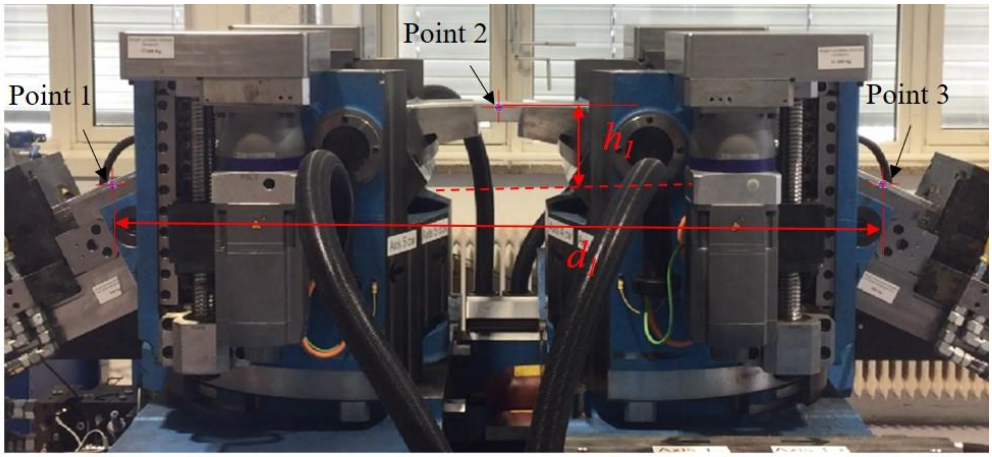

(a) Loading

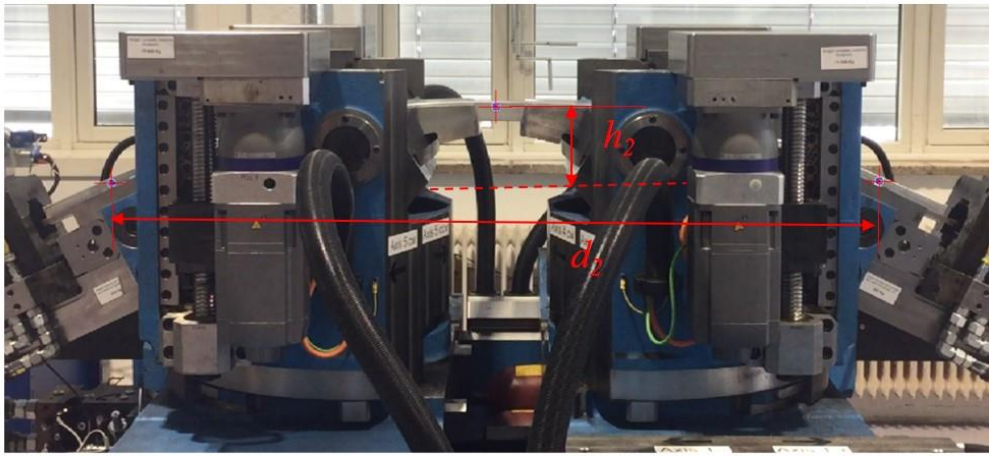

(b) Unloading

Figure 3.7. Original images of 50° bending

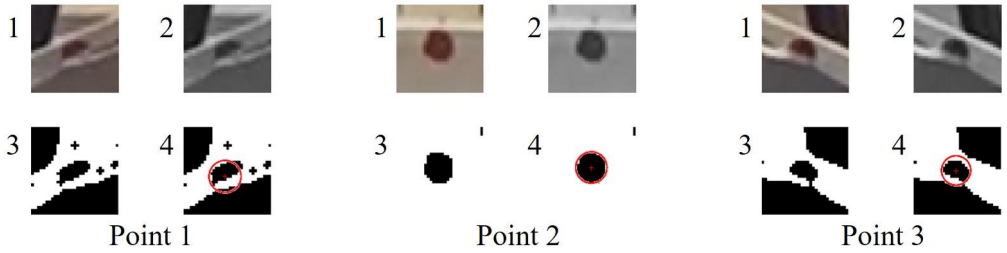

(a) Local circle search of a point after loading

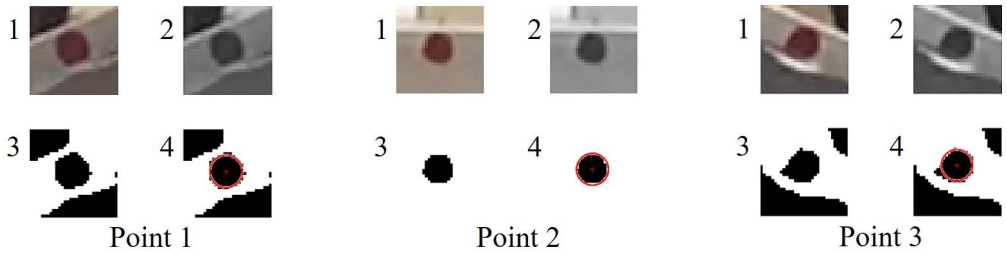

(b) Local circle search of a point after unloading

Figure 3.8. Image filtering and target detecting of 50° bending

The height between point 2 and a line passing through points 1 and 3 is changed after unloading, as shown in Figure 3.7. The height *h* is computed in the global coordinates given by

$$h = \frac{\left|(y_3 - y_1)(x_2 - x_1) + (x_3 - x_1)(y_1 - y_2)\right|}{\sqrt{(y_3 - y_1)^2 + (x_3 - x_1)^2}} \tag{3.6}$$

where *x* and *y* represent the coordinate of the point's center, and the subscript indicates the number of points. The springback Δh in Figure 3.9 is the change of a sagitta and computed with two different sagittas from the loading and unloading status, which is expressed as

$$\Delta h = h_1 - h_2 \tag{3.7}$$

3.4. Measurement validation

Two profiles were bent at 30° and 50° angles. To validate the proposed computer vision technique, measurement results by computer vision were compared with two manually measured profiles. Measurement by computer vision was validated with the measured data after unloading, since manual measurement was conducted with the profiles after springback. Figure 3.9 illustrates a scheme manual measurement for springback. A profile was supported at two datum points by a fixture, and a Vernier caliper was used to measure the height h_2 from the reference distance L. Intrados of the profile was measured, representing the surface of die contact. Since the radius of the bend die, approx. 1,807 mm, is relatively larger than the center of the reference points from the bottom in Figure 3.3, the reference points were used for springback measurement. As shown in Figure 3.9, springback was evaluated by the difference between the height, h_1 and h_2.

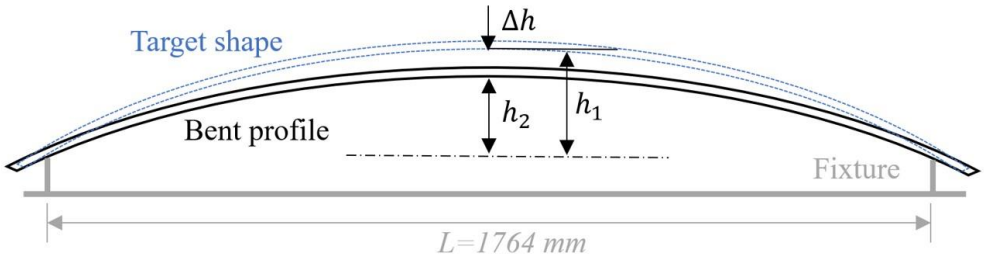

Figure 3.9. Scheme of springback measurement

The two profile samples of 30° and 50° bending are shown in Figure 3.10. Measured data after unloading by the computer vision and manual are listed in Table 3.2 and Table 3.3, respectively. In brief, the height in Table 3.2 and Table 3.3 increases as the bending angle increases, and the height becomes larger when the reference line increases. The reference points on a profile were predefined for image processing, and their location were changed during the bending cycle. Since the distance between points 1 and 3 was not the same as the fixture distance, *L=1764mm* in Table 3.3, measured data by the computer vision were converted to compare springback. Table 3.2 included raw data by the computer vision, and the converted data based on the fixture distance of manually measured profiles is listed in Table 3.4.

(a) 30° bending

(b) 50° bending

Figure 3.10. Bent profiles

Table 3.2. Measured data after unloading by the computer vision

No.	Bending angle	Distance between points 1 & 3 (d_2)	Height (h_2)
1	30°	1604.98 mm	51.78 mm
2	50°	1582.60 mm	156.05 mm

Table 3.3. Manually measured data

No.	Bending angle	Fixture distance (L)	Height (h_2)
1	30°	1764 mm	74.90 mm
2	50°	1764 mm	196.50 mm

Manual springback measurements and the ones by computer vision are compared in Table 3.4. The reference distances between points 1 and 2, 1604.98 mm for 30° bending and 1582.60 mm for 50° bending, were converted to 1764 mm. The cord heights of 30° bending by the computer vision and manual were 72.70 mm and 74.90 mm, respectively. While the relative difference was 2.77 %, the absolute difference of springback was 2.20 mm. For 50° bending, each chord height obtained by computer vision and manual was 197.98 mm and 196.50 mm, respectively, meaning that the relative difference was 0.71 %. The absolute difference of springback was 1.48 mm, which was less than the difference of 30° bending. According to a dimensional tolerance, the dimensional quality of the difference values, 2.20mm and 1.48mm, is determined. While two samples are hardly justifiable to validate the measurement method, it shows potential of computer vision-based measuring for springback of large profiles.

Table 3.4. Results of the computer vision and manual measurement (unit: mm)

No.	Bending angle	Fixture distance (L)	Height (h_2)		Target height (h_1)	Springback (Δh)	
			Computer vision	Manual		Computer vision	Manual
1	30°	1764	72.70	74.90	79.31	6.71	4.41
2	50°	1764	197.98	196.50	207.84	10.05	11.34

3.5. Conclusions

In this paper, a computer vision technique was adopted to monitor springback and to overcome the challenge of range of a measuring device for a large profile. Two different bending cases with 30° and 50° angles were experimentally analyzed using AA6082 T-4 hollow profiles of 1,900 mm length. Using a laptop computer and a cell phone camera, springback was monitored during bending process without extra sensors or electronic components attached to the machine. Images obtained by a cell phone were processed by MATLAB, and the acquired images were segmented and filtered. The circular hough transform (CHT) algorithm was used to search reference points on the profile. With the detected points, springback was evaluated by calculating the Euclidean distance of the sagitta.

The measurement results were validated with the manually measured data. For the 30° and 50° bending, released profile chord heights were 51.78 mm and 156.05 mm. The distance between points 1 and 3 of an image was converted to 1,764 mm of the fixture distance for comparison. The relative springback difference by the computer vision was 2.77 % for 30° bending and 0.71 % for 50° bending compared to the manual measurements. Although the sample size was small, the computer vision technique under operation showed potential to measure springback in large-profile bending.

Sensor-based digital data is one of the essential elements to move forward to Industry 4.0 and digital transformation. The proposed measurement has the advantages of an affordable setup, non-contact sensing, and in-situ monitoring for a large-profile springback. It is expected to increase the performance of the computer vision technique in this study with the several factors, image quality with high resolution, reduction of image distortion, and precise marking of reference points.

4. On kinematics in sequential three-dimensional (3D) stretch bending: Analytical springback model[***]

Ha, Taekwang; Welo, Torgeir; Ringen, Geir; Wang, Jyhwen. On kinematics in sequential three-dimensional (3D) stretch bending: analytical springback model.

This paper is submitted for publication and is therefore not included.

[***] Submitted to Journal of Manufacturing Science and Engineering

5. Smart control of springback in advanced stretch bending by an artificial neural network[****]

Ha, Taekwang; Welo, Torgeir; Ringen, Geir; Wang, Jyhwen. Smart control of springback in advanced stretch bending by an artificial neural network.

This paper is submitted for publication and is therefore not included.

[****] Submitted to Journal of Manufacturing Processes

6. Conclusions and suggested future works

6.1. Conclusions

Many automakers try to minimize the number of components to increase fuel efficiency. Optimized manufacturing processes reduce manufacturing costs and improve productivity. In addition, complex shapes of products are consistently demanded due to design purposes or aesthetic views. Thus, light and high-strength materials, such as aluminum alloys, have been in the spotlight, and manufacturing processes such as bending have been widely used to satisfy industrial demands.

As manufacturing environments are becoming flexible and smart manufacturing is coming up for better productivity, manufacturing processes from upstream to downstream are required to be intimately connected and integrated. In this context, the main objectives of this dissertation are to measure and monitor springback in real time, and to predict and control springback in order to improve the dimensional accuracy of 2D and 3D profiles bent in stretch bending.

To accomplish the first research objective, measuring and monitoring springback in real time, on-machine measurement methods as non-contact methods are developed based on image processing and laser tracking. In Paper I, the laser tracking approach makes it possible to evaluate springback in rotary draw bending without taking the workpiece from the bending machine. In Paper II, the image processing to find reference points as location indicators enables measuring springback of a large profile in stretch bending. By conducting experiments, the developed methods are validated. Both measurement approaches show that the developed non-contact methods can be used for measuring and monitoring springback.

In Paper III, the kinematic model of the semidie and the analytical springback model are developed to achieve the second research objective—springback prediction in 3D stretch bending. The Frenet-Serret theorem is adopted to describe the various curvature of the 3D bent geometry. Experiments and numerical simulations are also used to demonstrate the springback prediction capability of the analytic model. In addition, the pre-stretch effect is also investigated in stretch bending. By evaluating the prediction capability, it is proved that the proposed method can predict 3D springback in stretch bending.

Paper IV addresses the third research objective—improvement of the dimensional accuracy. To achieve the objective, an ANN model is developed to control springback in stretch bending.

The proposed ANN model provides the adjusted bending angles to achieve the desired geometry. The controlled case by the ANN and the uncontrolled case are compared to demonstrate the improvement of geometrical accuracy. It is concluded that the ANN helps to control springback and improve dimensional accuracy. The springback control method can be integrated with the control system for better product quality toward Industry 4.0.

6.2. Future works

The current manufacturing environments have rapidly changed beyond automation, and better manufacturing flexibility, productivity, and efficiency are still of interest. In new manufacturing environments towards Industry 4.0, computer systems are connected, digital data are integrated, and decisions are made based on data-driven approaches. In this respect, the current work in bending can be improved as described below.

The digital-image based laser tracking method was proposed to monitor springback in rotary draw bending. The laser assembly was fit at the end of a profile, and the laser point was projected on the datum board. Since the laser spot exist within the datum board, measurable bending angles are limited. Using the grid or point pattern on the profile, the springback after bending may be accurately monitored regardless of bending angles, and deformation during and after bending can be investigated. Robust image-processing algorithms may be required to recognize the patterns; developing AI algorithms may be helpful to process a large amount of data and improve the image-processing speed.

In stretch bending, an in-situ monitoring method for springback was proposed. The measurement method was a non-contact method, and a mobile phone was used to acquire image data during processing. While the system was affordable and efficient in 2D stretch bending, it had some limitations: image distortion, low-quality image resolution, or incomplete reference points. The performance of the computer vision technique can be improved as follows: More accurate dimensions can be measured based on the accurate shape and location of reference points on a profile. Two image acquisition devices can help to identify 3D geometry instead of a single camera for 3D stretch bending. Moreover, developing an AI algorithm to recognize reference points will speed up image processing.

The 3D springback model proposed in this dissertation accounts for global deformation in advanced stretch bending. The global deformation was experimentally and numerically demonstrated. In advanced stretch bending, the die-pivot location for bending a profile affects the strain history during bending. Global deformation can be further investigated by changing the pivot location to bend a profile. Local deformation such as distortion or sagging, however, can be a defect to control product quality as well. Considering local deformation with respect to loading sequences in 3D stretch bending may improve the geometrical quality.

The springback control approach using an ANN was proposed to improve the geometrical quality of a profile. While the proposed ANN model was trained with experimental and

analytical data, nominal material properties and geometries of an aluminum alloy were considered without considering deviations. Using upstream material data, different material properties can be integrated into the prediction model. Deviations of the material properties and geometries can be considered by the processing data provided by the ANN, and the bending processes can be also controlled in real time.

References

[1] Definition of MANUFACTURING n.d. https://www.merriam-webster.com/dictionary/manufacturing (accessed October 8, 2022).

[2] Dursun T, Soutis C. Recent developments in advanced aircraft aluminium alloys. Mater Des 1980-2015 2014;56:862–71. https://doi.org/10.1016/j.matdes.2013.12.002.

[3] Cadillac CT6 Elevates the Science of Mass Efficiency. MediaGmCom 2015. https://media.gm.com/media/us/en/gm/news.detail.html/content/Pages/news/us/en/2015/mar/0313-cadillac-ct6.html.

[4] Shen H, Vollertsen F. Modelling of laser forming–An review. Comput Mater Sci 2009;46:834–40. https://doi.org/10.1016/j.commatsci.2009.04.022.

[5] Li W, Yao YL. Laser bending of tubes: mechanism, analysis, and prediction. J Manuf Sci Eng 2001;123:674–81. https://doi.org/10.1115/1.1392992.

[6] Miller G. Tube forming processes: a comprehensive guide. Society of Manufacturing Engineers; 2003.

[7] Paulsen F, Welo T, Søvik OP. A design method for rectangular hollow sections in bending. 5th Asia Pac Conf Mater Process 2001;113:699–704. https://doi.org/10.1016/S0924-0136(01)00671-9.

[8] Dyau JY, Kyriakides S. On the response of elastic-plastic tubes under combined bending and tension 1992. https://doi.org/10.1115/1.2919952.

[9] Clausen AH, Hopperstad OS, Langseth M. Stretch bending of aluminum extrusions: effect of geometry and alloy. J Eng Mech 1999;125:392–400. https://doi.org/10.1061/(ASCE)0733-9399(1999)125:4(392).

[10] Welo T, Granly B. A new adaptive bending method using closed loop feedback control. Trans Nonferrous Met Soc China 2010;20:2111–7. https://doi.org/10.1016/S1003-6326(09)60426-X.

[11] Karafillis AP, Boyce MC. Tooling design in sheet metal forming using springback calculations. Int J Mech Sci 1992;34:113–31. https://doi.org/10.1016/0020-7403(92)90077-T.

[12] Gan W, Wagoner RH. Die design method for sheet springback. Int J Mech Sci 2004;46:1097–113. https://doi.org/10.1016/j.ijmecsci.2004.06.006.

[13] Wang H, Zhou J, Zhao T, Tao Y. Springback compensation of automotive panel based on three-dimensional scanning and reverse engineering. Int J Adv Manuf Technol 2016;85:1187–93. https://doi.org/10.1007/s00170-015-8042-x.

[14] Rosenblatt F. The perceptron: a probabilistic model for information storage and organization in the brain. Psychol Rev 1958;65:386–408. https://doi.org/10.1037/h0042519.

[15] Aggarwal CC. Neural networks and deep learning. vol. 10. Springer; 2018.

[16] Wang Q, Ma Y, Zhao K, Tian Y. A Comprehensive Survey of Loss Functions in Machine Learning. Ann Data Sci 2022;9:187–212. https://doi.org/10.1007/s40745-020-00253-5.

[17] Alwosheel A, van Cranenburgh S, Chorus CG. Is your dataset big enough? Sample size requirements when using artificial neural networks for discrete choice analysis. J Choice Model 2018;28:167–82. https://doi.org/10.1016/j.jocm.2018.07.002.

[18] Shtub A, Versano R. Estimating the cost of steel pipe bending, a comparison between neural networks and regression analysis. Int J Prod Econ 1999;62:201–7. https://doi.org/10.1016/S0925-5273(98)00212-6.

[19] Haghdadi N, Zarei-Hanzaki A, Khalesian AR, Abedi HR. Artificial neural network modeling to predict the hot deformation behavior of an A356 aluminum alloy. Mater Des 2013;49:386–91. https://doi.org/10.1016/j.matdes.2012.12.082.

[20] Hsiang S-H, Kuo J-L, Yang F-Y. Using artificial neural networks to investigate the influence of temperature on hot extrusion of AZ61 magnesium alloy. J Intell Manuf 2006;17:191–201. https://doi.org/10.1007/s10845-005-6636-0.

[21] Shahin M, Elchalakani M. Neural networks for modelling ultimate pure bending of steel circular tubes. J Constr Steel Res 2008;64:624–33. https://doi.org/10.1016/j.jcsr.2007.12.001.

[22] D'Aniello M, Güneyisi EM, Landolfo R, Mermerdaş K. Predictive models of the flexural overstrength factor for steel thin-walled circular hollow section beams. Thin-Walled Struct 2015;94:67–78. https://doi.org/10.1016/j.tws.2015.03.020.

[23] Ruffini R, Cao J. Using Neural Network for Springback Minimization in a Channel Forming Process. SAE Trans 1998;107:65–73.

[24] Manabe K sa, Yang M, Yoshihara S. Artificial intelligence identification of process parameters and adaptive control system for deep-drawing process. J Mater Process Technol 1998;80:421–6.

[25] Lin JC, Tai CC. The application of neural networks in the prediction of spring-back in an L-shaped bend. Int J Adv Manuf Technol 1999;15:163–70. https://doi.org/10.1007/s001700050053.

[26] Ma J, Li H, Chen GY, Welo T, Li GJ. Machine Learning (ML)-Based Prediction and Compensation of Springback for Tube Bending. In: Daehn G, Cao J, Kinsey B, Tekkaya E, Vivek A, Yoshida Y, editors. Form. Future, Cham: Springer International Publishing; 2021, p. 167–78. https://doi.org/10.1007/978-3-030-75381-8_13.

[27] Zhong RY, Xu X, Klotz E, Newman ST. Intelligent Manufacturing in the Context of Industry 4.0: A Review. Engineering 2017;3:616–30. https://doi.org/10.1016/J.ENG.2017.05.015.

[28] Allwood JM, Duncan SR, Cao J, Groche P, Hirt G, Kinsey B, et al. Closed-loop control of product properties in metal forming. CIRP Ann 2016;65:573–96. https://doi.org/10.1016/j.cirp.2016.06.002.

[29] Löbbe C, Hoppe C, Becker C, Tekkaya AE. Closed loop springback control in progressive die bending by induction heating. Int J Precis Eng Manuf 2015;16:2441–9. https://doi.org/10.1007/s12541-015-0314-8.

[30] Pan K, Stelson KA. On the plastic deformation of a tube during bending. J Eng Ind 1995;117:494–500. https://doi.org/10.1115/1.2803526.

[31] Borchmann L, Kuhnhen C, Frohn P, Engel B. Sensitivity analysis of the rotary draw bending process as a database of digital equipping support. Procedia Manuf 2019;29:592–9. https://doi.org/10.1016/j.promfg.2019.02.100.

[32] Garcia-Romeu ML, Ciurana J, Ferrer I. Springback determination of sheet metals in an air bending process based on an experimental work. J Mater Process Technol 2007;191:174–7. https://doi.org/10.1016/j.jmatprotec.2007.03.019.

[33] Wang J, Verma S, Alexander R, Gau J-T. Springback control of sheet metal air bending process. J Manuf Process 2008;10:21–7. https://doi.org/10.1016/j.manpro.2007.09.001.

[34] Inamdar MV, Date PP, Desai UB. Studies on the prediction of springback in air vee bending of metallic sheets using an artificial neural network. J Mater Process Technol 2000;108:45–54. https://doi.org/10.1016/S0924-0136(00)00588-4.

[35] Ghiotti A, Simonetto E, Bruschi S, Bariani PF. Springback measurement in three roll push bending process of hollow structural sections. CIRP Ann 2017;66:289–92. https://doi.org/10.1016/j.cirp.2017.04.119.

[36] Katona S, Lušić M, Koch M, Wartzack S. Integrating optical 3D measurement techniques in pipe bending: a model-based approach minimizing waste by deriving real functional design behaviour. Procedia CIRP 2016;50:808–12. https://doi.org/10.1016/j.procir.2016.04.163.

[37] Lau K, Hocken R, Haynes L. Robot performance measurements using automatic laser tracking techniques. Robot Comput-Integr Manuf 1985;2:227–36. https://doi.org/10.1016/0736-5845(85)90110-3.

[38] Ha T, Ma J, Blindheim J, Welo T, Ringen G, Wang J. In-line Springback Measurement for Tube Bending Using a Laser System. Procedia Manuf 2020;47:766–73. https://doi.org/10.1016/j.promfg.2020.04.233.

[39] Solomon C, Breckon T. Fundamentals of Digital Image Processing: A practical approach with examples in Matlab. John Wiley & Sons; 2011.

[40] Ferreira JA, Sun P, Grácio JJ. Close loop control of a hydraulic press for springback analysis. J Mater Process Technol 2006;177:377–81. https://doi.org/10.1016/j.jmatprotec.2006.03.177.

[41] Pratt WK. Digital image processing. Wiley-Interscience, New York; 2007.

[42] Sahoo PK, Soltani S, Wong AK. A survey of thresholding techniques. Comput Vis Graph Image Process 1988;41:233–60. https://doi.org/10.1016/0734-189X(88)90022-9.

[43] Piccardi M. Background subtraction techniques: a review. 2004 IEEE Int. Conf. Syst. Man Cybern. IEEE Cat No04CH37583, vol. 4, 2004, p. 3099–104. https://doi.org/10.1109/icsmc.2004.1400815.

[44] Sen-Ching SC, Kamath C. Robust techniques for background subtraction in urban traffic video. Vis. Commun. Image Process. 2004, vol. 5308, International Society for Optics and Photonics; 2004, p. 881–92. https://doi.org/10.1117/12.526886.

[45] Pal NR, Pal SK. A review on image segmentation techniques. Pattern Recognit 1993;26:1277–94. https://doi.org/10.1016/0031-3203(93)90135-J.

[46] Yilmaz A, Javed O, Shah M. Object tracking: A survey. Acm Comput Surv CSUR 2006;38:13-es. https://doi.org/10.1145/1177352.1177355.

[47] Welo T, Ringen G, Ma J. An overview and evaluation of alternative forming processes for complex aluminium products. Procedia Manuf 2020;48:82–9. https://doi.org/10.1016/j.promfg.2020.05.022.

[48] Ma J, Welo T. Analytical springback assessment in flexible stretch bending of complex shapes. Int J Mach Tools Manuf 2020:103653.

[49] Hamedon Z, Mori K, Abe Y. In-situ measurement of three-dimensional deformation behaviour of sheet and tools during stamping using borescope. J Mater Process Technol 2014;214:945–50. https://doi.org/10.1016/j.jmatprotec.2013.11.016.

[50] Ferreira JA, Sun P, Grácio JJ. Close loop control of a hydraulic press for springback analysis. J Mater Process Technol 2006;177:377–81. https://doi.org/Elsevier Journal of Materials Processing Technology Volume 177, Issues 1–3, 3 July 2006, Pages 377-381 Journal of Materials Processing Technology Close loop control of a hydraulic press for springback analysis Author links open overlay panelJ.A.FerreiraP.SunJ.J.Grácio https://doi.org/10.1016/j.jmatprotec.2006.03.177.

[51] Corona E. A simple analysis for bend-stretch forming of aluminum extrusions. Int J Mech Sci 2004;46:433–48. https://doi.org/10.1016/j.ijmecsci.2004.03.010.

[52] Clausen Arild H., Hopperstad Odd S., Langseth Magnus. Stretch Bending of Aluminum Extrusions: Effect of Tensile Sequence. J Eng Mech 1999;125:521–9. https://doi.org/10.1061/(ASCE)0733-9399(1999)125:5(521).

[53] Gunasekaran S. Computer vision technology for food quality assurance. Trends Food Sci Technol 1996;7:245–56. https://doi.org/10.1016/0924-2244(96)10028-5.

[54] Beymer D, McLauchlan P, Coifman B, Malik J. A real-time computer vision system for measuring traffic parameters. Proc. IEEE Comput. Soc. Conf. Comput. Vis. Pattern Recognit., 1997, p. 495–501. https://doi.org/10.1109/CVPR.1997.609371.

[55] Geiger A, Lenz P, Urtasun R. Are we ready for autonomous driving? the kitti vision benchmark suite. 2012 IEEE Conf. Comput. Vis. Pattern Recognit., IEEE; 2012, p. 3354–61. https://doi.org/10.1109/CVPR.2012.6248074.

[56] Matthies L, Maimone M, Johnson A, Cheng Y, Willson R, Villalpando C, et al. Computer vision on Mars. Int J Comput Vis 2007;75:67–92. https://doi.org/10.1007/s11263-007-0046-z.

[57] Wahbeh AM, Caffrey JP, Masri SF. A vision-based approach for the direct measurement of displacements in vibrating systems. Smart Mater Struct 2003;12:785.

[58] Fukuda Y, Feng MQ, Shinozuka M. Cost-effective vision-based system for monitoring dynamic response of civil engineering structures. Struct Control Health Monit 2010;17:918–36.

[59] Pan B, Qian K, Xie H, Asundi A. Two-dimensional digital image correlation for in-plane displacement and strain measurement: a review. Meas Sci Technol 2009;20:062001.

[60] Duda RO, Hart PE. Use of the Hough transformation to detect lines and curves in pictures. Commun ACM 1972;15:11–5.

[61] Kimme C, Ballard D, Sklansky J. Finding circles by an array of accumulators. Commun ACM 1975;18:120–2.

[62] Rosenthal S, Maaß F, Kamaliev M, Hahn M, Gies S, Tekkaya AE. Lightweight in Automotive Components by Forming Technology. Automot Innov 2020;3:195–209. https://doi.org/10.1007/s42154-020-00103-3.

[63] Hirsch J. Recent development in aluminium for automotive applications. Trans Nonferrous Met Soc China 2014;24:1995–2002. https://doi.org/10.1016/S1003-6326(14)63305-7.

[64] Benedyk JC. Aluminum alloys for lightweight automotive structures. In: Mallick PK, editor. Mater. Des. Manuf. Lightweight Veh., Woodhead Publishing; 2010, p. 79–113.

[65] Vollertsen F, Sprenger A, Kraus J, Arnet H. Extrusion, channel, and profile bending: a review. J Mater Process Technol 1999;87:1–27. https://doi.org/10.1016/S0924-0136(98)00339-2.

[66] Brazier LG. On the flexure of thin cylindrical shells and other" thin" sections. Proc R Soc Lond Ser Contain Pap Math Phys Character 1927;116:104–14. https://doi.org/10.1098/rspa.1927.0125.

[67] Paulsen F, Welo T. 3D Bending of Aluminium Extrusions for Automotive Applications. Warrendale, PA: SAE International; 2003. https://doi.org/10.4271/2003-01-2855.

[68] Paulsen F, Welo T. A design method for prediction of dimensions of rectangular hollow sections formed in stretch bending. J Mater Process Technol 2002;128:48–66. https://doi.org/10.1016/S0924-0136(02)00178-4.

[69] Baba A, Tozawa Y. Effect of tensile force in stretch-forming process on the springback. Bull JSME 1964;7:834–43. https://doi.org/10.1299/jsme1958.7.834.

[70] Kuwabara T, Takahashi S, Akiyama K, Miyashita Y. 2-D Springback Analysis for Stretch-Bending Processes Based on Total Strain Theory. SAE Trans 1995;104:504–13.

[71] Ueda M, Ueno K, Kobayashi M. A study of springback in the stretch bending of channels. J Mech Work Technol 1981;5:163–79. https://doi.org/10.1016/0378-3804(81)90038-3.

[72] Yu TX, Johnson W. Influence of axial force on the elastic-plastic bending and springback of a beam. J Mech Work Technol 1982;6:5–21. https://doi.org/10.1016/0378-3804(82)90016-X.

[73] El-Domiaty A, Shabaik AH. Bending of work-hardening metals under the influence of axial load. J Mech Work Technol 1984;10:57–66. https://doi.org/10.1016/0378-3804(84)90078-0.

[74] El-Domiaty A. Stretch forming of beams of non-uniform section. J Mater Process Technol 1990;22:21–8. https://doi.org/10.1016/0924-0136(90)90139-L.

[75] El-Domiaty AA, Elsharkawy AA. Stretch-bending analysis of U-section beams. Int J Mach Tools Manuf 1998;38:75–95. https://doi.org/10.1016/S0890-6955(97)00008-4.

[76] Clausen AH, Hopperstad OS, Langseth M. Sensitivity of model parameters in stretch bending of aluminium extrusions. Int J Mech Sci 2001;43:427–53. https://doi.org/10.1016/S0020-7403(00)00012-6.

[77] Miller JE, Kyriakides S, Bastard AH. On bend-stretch forming of aluminum extruded tubes—I: experiments. Int J Mech Sci 2001;43:1283–317. https://doi.org/10.1016/S0020-7403(00)00039-4.

[78] Zhu H, Stelson KA. Distortion of rectangular tubes in stretch bending. J Manuf Sci Eng 2002;124:886–90. https://doi.org/10.1115/1.1511170.

[79] Miller JE, Kyriakides S. Three-dimensional effects of the bend–stretch forming of aluminum tubes. Int J Mech Sci 2003;45:115–40. https://doi.org/10.1016/S0020-7403(03)00036-5.

[80] Paulsen F, Welo T. Cross-sectional deformations of rectangular hollow sections in bending: Part I — experiments. Int J Mech Sci 2001;43:109–29. https://doi.org/10.1016/S0020-7403(99)00106-X.

[81] Paulsen F, Welo T. Cross-sectional deformations of rectangular hollow sections in bending: Part II — analytical models. Int J Mech Sci 2001;43:131–52. https://doi.org/10.1016/S0020-7403(99)00107-1.

[82] Welo T, Baringbing HA. On the evaluation of dimensional accuracy in rotary stretch bending. Int J Mater Form 2009;2:849. https://doi.org/10.1007/s12289-009-0642-2.

[83] Ma J, Welo T, Blindheim J, Ha T. Effect of Stretching on Springback in Rotary Stretch Bending of Aluminium Alloy Profiles. Key Eng. Mater., vol. 883, Trans Tech Publ; 2021, p. 175–80. https://doi.org/10.4028/www.scientific.net/KEM.883.175.

[84] Ma J, Welo T. Analytical springback assessment in flexible stretch bending of complex shapes. Int J Mach Tools Manuf 2021;160:103653. https://doi.org/10.1016/j.ijmachtools.2020.103653.

[85] Liang J, Gao S, Teng F, Yu P, Song X. Flexible 3D stretch-bending technology for aluminum profile. Int J Adv Manuf Technol 2014;71:1939–47. https://doi.org/10.1007/s00170-013-5590-9.

[86] Liang J, Chen C, Li Y, Liang C. Effect of roller dies on springback law of profile for flexible 3D multi-point stretch bending. Int J Adv Manuf Technol 2020;108:3765–77. https://doi.org/10.1007/s00170-020-05655-6.

[87] Welo T, Ma J, Blindheim J, Ha T, Ringen G. Flexible 3D stretch bending of aluminium alloy profiles: an experimental and numerical study. Procedia Manuf 2020;50:37–44. https://doi.org/10.1016/j.promfg.2020.08.008.

[88] Millman RS, Parker GD. Elements of differential geometry. Prentice-Hall Englewood Cliffs, NJ; 1977.

[89] Ha T, Welo T, Ringen G, Wang J. A strategy for on-machine springback measurement in rotary draw bending using digital image-based laser tracking. Int J Adv Manuf Technol 2022;119:705–18. https://doi.org/10.1007/s00170-021-08178-w.

[90] Ha T, Ma J, Blindheim J, Welo T, Ringen G, Wang J. A computer vision-based, in-situ springback monitoring technique for bending of large profiles. ESAFORM 2021, Liège, Belgique: ULiège Library; 2021. https://10.25518/esaform21.4002.

[91] Davis J. The Potential for Vehicle Weight Reduction Using Magnesium. Warrendale, PA: SAE International; 1991. https://doi.org/10.4271/910551.

[92] Schneider SH, Moya S, v.N. Whitman M. Global warming. Issues Sci Technol 1989;6:23–5.

[93] Leduc P, Dubar B, Ranini A, Monnier G. Downsizing of gasoline engine: an efficient way to reduce CO2 emissions. Oil Gas Sci Technol 2003;58:115–27.

[94] Hucho W-H. Aerodynamics of Road Vehicles: From Fluid Mechanics to Vehicle Engineering. Elsevier; 2013.

[95] Wood RM. Impact of Advanced Aerodynamic Technology on Transportation Energy Consumption. SAE Trans 2004;113:854–74.

[96] Koffler C, Rohde-Brandenburger K. On the calculation of fuel savings through lightweight design in automotive life cycle assessments. Int J Life Cycle Assess 2009;15:128. https://doi.org/10.1007/s11367-009-0127-z.

[97] Han HN, Clark JP. Lifetime costing of the body-in-white: Steel vs. aluminum. JOM 1995;47:22–8. https://doi.org/10.1007/BF03221171.

[98] He Y, Heng L, Zhang Z, Mei Z, Jing LIU, Guangjun L. Advances and trends on tube bending forming technologies. Chin J Aeronaut 2012;25:1–12. https://doi.org/10.1016/S1000-9361(11)60356-7.

[99] Elsharkawy AA, El-Domiaty AA. Determination of stretch-bendability limits and springback for T-section beams. J Mater Process Technol 2001;110:265–76. https://doi.org/10.1016/S0924-0136(00)00885-2.

[100] Liu T, Wang Y, Wu J, Xia X, Wang J, Wang W, et al. Springback analysis of Z & T-section 2196-T8511 and 2099-T83 Al–Li alloys extrusions in displacement controlled cold stretch bending. J Mater Process Technol 2015;225:295–309. https://doi.org/10.1016/j.jmatprotec.2015.05.024.

[101] Gu Z, Lv M, Li X, Xu H. Stretch bending defects control of L-section aluminum components with variable curvatures. Int J Adv Manuf Technol 2016;85:1053–61. https://doi.org/10.1007/s00170-015-8010-5.

[102] Welo T, Widerøe F. Precision bending of high-quality components for volume applications. Trans Nonferrous Met Soc China 2010;20:2100–10. https://doi.org/10.1016/S1003-6326(09)60425-8.

[103] Cao J, Kinsey B, Solla SA. Consistent and Minimal Springback Using a Stepped Binder Force Trajectory and Neural Network Control. J Eng Mater Technol 1999;122:113–8. https://doi.org/10.1115/1.482774.

[104] Sunseri M, Cao J, Karafillis AP, Boyce MC. Accommodation of Springback Error in Channel Forming Using Active Binder Force Control: Numerical Simulations and Experiments. J Eng Mater Technol 1996;118:426–35. https://doi.org/10.1115/1.2806830.

[105] Liu W, Liu Q, Ruan F, Liang Z, Qiu H. Springback prediction for sheet metal forming based on GA-ANN technology. J Mater Process Technol 2007;187:227–31. https://doi.org/10.1016/j.jmatprotec.2006.11.087.

[106] Geiger M, Sprenger A. Controlled Bending of Aluminium Extrusions. CIRP Ann 1998;47:197–202. https://doi.org/10.1016/S0007-8506(07)62817-0.

[107] Smith S. Digital signal processing: a practical guide for engineers and scientists. Elsevier; 2003.

[108] Burden F, Winkler D. Bayesian regularization of neural networks. Methods Mol Biol Clifton NJ 2008;458:25–44. https://doi.org/10.1007/978-1-60327-101-1_3.

[109] Dan Foresee F, Hagan MT. Gauss-Newton approximation to Bayesian learning. Proc. Int. Conf. Neural Netw. ICNN97, vol. 3, 1997, p. 1930–5 vol.3. https://doi.org/10.1109/ICNN.1997.614194.

ISBN 978-82-326-6275-3 (printed ver.)
ISBN 978-82-326-5601-1 (electronic ver.)
ISSN 1503-8181 (printed ver.)
ISSN 2703-8084 (online ver.)

NTNU

Norwegian University of
Science and Technology